5-2018

Quantifying Carbon and Water Dynamics of Terrestrial Ecosystems At High Temporal And Spatial Resolutions Using Process-Based Biogeochemistry Models And In Situ And Satellite Data

Yang Qu
Purdue University

QUANTIFYING CARBON AND WATER DYNAMICS OF TERRESTRIAL ECOSYSTEMS AT HIGH TEMPORAL AND SPATIAL RESOLUTIONS USING PROCESS-BASED BIOGEOCHEMISTRY MODELS AND IN SITU AND SATELLITE DATA

by

Yang Qu

A Dissertation

Submitted to the Faculty of Purdue University

In Partial Fulfillment of the Requirements for the degree of

Doctor of Philosophy

Department of Earth, Atmospheric, & Planetary Sciences

West Lafayette, Indiana

May 2018

THE PURDUE UNIVERSITY GRADUATE SCHOOL
STATEMENT OF COMMITTEE APPROVAL

Dr. Qianlai Zhuang, Chair

School of Earth, Atmospheric, & Planetary Sciences

Dr. Hao Zhang

School of Statistics

Dr. Yutian Wu

School of Earth, Atmospheric, & Planetary Sciences

Dr. Harshvardhan

School of Earth, Atmospheric, & Planetary Sciences

Approved by:

Dr. Indrajeet Chaubey

Head of the Graduate Program

In Dedication to My Parents and Best Friends

ACKNOWLEDGMENTS

Firstly, I want to express my sincere appreciation to my Advisor Dr. Qianlai Zhuang, for his continuous encouragement, patience, and support, helping me overcome difficulties toward my dissertation research. I also want to give my deep gratitude to my committee members: Dr. Harshvardhan, Dr. Hao Zhang and Dr. Yutian Wu, for their constructive comments and suggestions during my PhD period. My advisor and all committee members are thought-provoking, improved me to a high research standard. I am grateful for them to comment on thesis and presentations.

I am also grateful to every member of our lab EBDL (Ecosystems & Biogeochemical Dynamics Laboratory) in EAPS at Purdue, for their guidance and assistance. Their support is not only technical but also providing a warm atmosphere in the lab.

I also want to thank all the faculty members for their help and support of the EAPS. Especially, I would like to thank the ITaP staff who maintained the software and hardware in our lab. Last but not the least, I would like to thank Purdue RCAC for their continuous support of cluster resources, which provide fundamental computing resources for my research.

TABLE OF CONTENTS

LIST OF TABLES

LIST OF FIGURES

ABSTRACT

Author: Qu, Yang. PhD
Institution: Purdue University
Degree Received: May 2018
Title: Quantifying Carbon and Water Dynamics of Terrestrial Ecosystems At High Temporal And Spatial Resolutions Using Process-Based Biogeochemistry Models And In Situ And Satellite Data
Major Professor: Qianlai Zhuang

To better understand the role of terrestrial ecosystems in the global carbon cycle and their feedbacks to the global climate system, process-based ecosystem models that are used for quantifying net carbon exchanges between the terrestrial biosphere and the atmosphere need to be improved. My research objective is to improve the model from following aspects: 1) Improving parameterization and model structure for carbon and water dynamics, 2) improving regional model simulations at finer spatial resolutions (from 0.5 degree to 0.05 degree or finer), 3) developing faster spin-up algorithms, and 4) evaluating high performance model simulations using fast spin-up technique deployed on various computing platforms. I improved the leaf area index (LAI) modeling in a terrestrial ecosystem model (TEM) for North America. The evaluated TEM was used to estimate ET at site and regional scales in North America from 2000 to 2010. The estimated annual ET varies from 420 to 450 mm yr^{-1} with the improved model, close to MODIS monthly data with root-mean-square-error less than 10 mm□month-1 for the study period. Alaska, Canada, and the conterminous US accounts for 33%, 6% and 61% of the regional ET, respectively. I then used new algorithm for a fast spin-up for TEM. With the new spin-up algorithm, I showed that the model reached a steady state in less than 10 years of simulation time, while the original method requires more than 200 years on average of model run. Lastly, I conducted simulations under both original resolution and high resolution in the conterminous

US. The high-resolution simulation predicts slightly higher average annual gross primary production (GPP) (~2%) from 2000 to 2015 in the conterminous US than original version of TEM. From the improved TEM simulation, I estimated that regional GPP is between 7.12 and 7.69 Pg C yr^{-1} and NEP is between 0.09 and 0.75 Pg C yr^{-1}.

CHAPTER 1. INTRODUCTION

There is a large uncertainty in carbon-climate feedbacks within the global climate system models. To constrain the uncertainty, the terrestrial ecosystem carbon dynamics in the global carbon cycle and their feedbacks to the global climate system shall be improved. Specifically, the process-based biogeochemistry models used to quantify carbon dynamics need to be improved with respect to their parameterization and structure. To achieve these improvements, we need to not only improve the quantification of certain variables (e.g., Leaf Area Index, LAI) in process-based biogeochemistry models, but also develop new techniques (e.g., speed up simulations) to allow these models adapt for much finer spatial and temporal resolutions.

In this dissertation, my first study (Chapter 2) is to model a vegetation index, the Leaf Area Index (LAI), which is important to modeling ecosystem fluxes of carbon, water, and energy. LAI is often used to quantify plant production and evapotranspiration with terrestrial ecosystem models. This study evaluated the LAI simulation in North America using a data assimilation technique and a process-based terrestrial ecosystem model as well as *in situ* and satellite data. The interaction between biosphere and the atmosphere is strongly influenced by plant leaf phenology that refers to the temporal pattern of seasonal leaf onset and senescence (Arora & Boer 2005, Fisher el al. 2006). Under warming conditions, increasing greenhouse gas is expected to extend the growing season of plant leaf (Beaubien & Freeland 2000, Menzel & Fabian 1999, Chmielewski & Rötzer 2001). However, estimating leaf phenology with ecosystem models is still challenging although progress has been made in understanding the drivers of leaf phenology even at the molecular level (Sung & Amasino 2004). In the absence of process-based modeling of leaf phenology, empirical approaches in ecosystem and dynamic vegetation models have been tested with varying degrees of success (Linkosalo et al. 2008). However, TEM's capability to simulate

LAI has not yet been evaluated with observed data. Here we take advantage of available site-level and satellite-based observation data to fully evaluate TEM. We then conduct LAI simulations for natural ecosystems in North America. The remote sensing products for the entire region and various plant function types (PFTs) are used to evaluate the model. The changes of leaf phenology are then analyzed using LAI data for North America during the period of 1985-2010. This study focuses on improving quantification of LAI as an indicator of leaf phenology. We expect the correctly-modeled LAI and leaf phenology will improve quantification of ecosystem water, energy, and carbon dynamics.

With the improved LAI, I expect the quantification of evapotranspiration (ET) could be improved to better understand its role in the global hydrological cycle of terrestrial ecosystems and feedbacks to the climate system. To test that, my second study is to incorporate LAI to ET modeling (Chapter 3). Evapotranspiration (ET) is an important water flux in the terrestrial ecosystem hydrological cycle (Dolman & De Jeu, 2010) and is also a key energy flux of the land surface. ET links the atmosphere and ecosphere through the energy exchange and biogeochemical cycles (Betts et al., 1996; Mu et al., 2007; Sun et al., 2011; Katul et al., 2012). Different models showed that 60~67% of annual precipitation returns as ET to the atmosphere (Vörösmarty et al., 1998; Miralles et al., 2011; Zhang et al., 2016). The response of ET to increasing temperature and greenhouse gas concentrations will impact the climate system and water availability to human system. Accurate quantification of ET is important to estimating regional water balance and water availability, an important ecosystem service (Mooney et al., 2005) and conducting economic analysis (Vörösmarty et al., 2010).

To adequately quantify regional ET across space and time, terrestrial ecosystem models with well-constrained parameters using observed data are needed. Currently, ET quantification

still has large uncertainties due to uncertain forcing data and inadequate representation of the physical processes in the models (Liu et al., 2015). The uncertainties come from different environmental factors including plant phenology, soil moisture, solar radiation, temperature and wind speed. Previous quantification of ET in North America suffered from using a limited amount of in situ data of ET for model parameterization and verification (Liu et al., 2014).

In Chapter 3, I improved ET quantification in North America using a data assimilation technique and a process-based terrestrial ecosystem model as well as *in situ* and satellite data. ET is modeled using the Penman-Monteith equation with an improved leaf area index (LAI) algorithm in a biogeochemistry model, the Terrestrial Ecosystem Model (TEM). The evaluated TEM was used to estimate ET at site and regional scales in North America from 2000 to 2010. The estimated annual ET varies from 420 to 450 $mm \cdot yr^{-1}$ with the improved model, close to MODIS monthly data with root-mean-square-error less than 10 $mm \cdot month^{-1}$ for the study period.

To conduct process-based biogeochemistry models at finer resolutions, the spin-up time for those differential equation-based models needs to be shortened. Thus, my third study developed an algorithm for a fast spin-up, which was implemented in a biogeochemistry model, the Terrestrial Ecosystem Model (TEM) (Chapter 4). With the new spin-up algorithm, I showed that the model reached a steady state in less than 10 years equivalent of simulation time, while the original method requires more than 200 years on average of model run. For the test sites with five different plant function types, the new method saves over 90% of the original spin-up time in site-level simulations. In North America simulations, average spin-up time saving for all grid cells is 85% for either daily or monthly version of TEM. The developed spin-up method shall greatly facilitate our future quantification of carbon dynamics at fine spatial and temporal scales.

In Chapter 5, I used the fast spin-up method to conduct carbon simulations at finer spatial and temporal resolutions with TEM. Model spin-up is a step to get biogeochemistry models to a steady state for those state and flux variables (McGuire et al., 1992; King, 1995; Johns et al., 1997; Dickinson et al., 1998). Spin-up normally uses cyclic forcing data to force the model run, and reach a steady state, which will be used as initial conditions for model transient simulations. The steady state is reached when modeled state variables show a cyclic pattern or a constant and often requires a significant amount of computation time, which needs to be accelerated for regional and global simulations at fine spatial and temporal scales. With improved LAI and spin-up process in biogeochemistry models, I increased the spatial resolutions from 0.5 degree to 0.05 degree for carbon simulations. I found that the overall high-resolution TEM predicts slightly higher average annual GPP (~2%) from 2000-2015 in conterminous US than original version of TEM.

In final Chapter, I summarized my findings and envisioned potential next steps based on my dissertation research.

CHAPTER 2. MODELING LEAF AREA INDEX IN NORTH AMERICA USING A PROCESS-BASED TERRESTRIAL ECOSYSTEM MODEL

2.1 Abstract

Leaf area index (LAI) is often used to quantify plant production and evapotranspiration with terrestrial ecosystem models. This study evaluated the LAI simulation in North America using a data assimilation technique and a process-based terrestrial ecosystem model as well as *in situ* and satellite data. We first optimized the parameters related to LAI in the Terrestrial Ecosystem Model (TEM) using a Markov Chain Monte Carlo method, and AmeriFlux site-level and regional LAI data from AVHRR (Advanced Very High Resolution Radiometer). The parameterized model was then verified with the observed monthly LAI of major ecosystem types at site-level. Simulated LAI was compared well with the observed data at sites of Harvard Forest (R^2=0.96), University of Michigan Biological Station (UMBS) (R^2=0.87), Howland Forest (R^2=0.96), Morgan Monroe State Forest (R^2=0.85), Shidler Tallgrass Prairie (R^2=0.82), and Donaldson (R^2=0.75). The root-mean-square error (RMSE) between modeled and satellite-based monthly LAI in North America is 1.4 m^2m^{-2} for the period of 1985-2010. The simulated average monthly LAI in recent three decades increased by (3±0.5)% in the region, with 1.24, 1.46 and 2.21 m^2m^{-2} on average, in Alaska, Canada, and the conterminous US, respectively, which is consistent with satellite data. The model performed well for wet tundra, boreal forest, temperate coniferous forests, temperate deciduous forests, grasslands and xeric shrublands (*RMSE*<1.5 m^2m^{-2}), but not for alpine tundra and xeric woodlands (*RMSE*>1.5 m^2m^{-2}). Both the spring and fall LAI in the 2000s are higher than that in the 1980s in the region, suggesting that the leaf phenology has an earlier onset and later senescence in the 2000s. The average LAI increased in April and

September by 0.03 and 0.24 m^2m^{-2}, respectively. This study provides a way to quantify LAI with ecosystem models, which will improve future carbon and water cycling studies.

2.2 Introduction

The interaction between biosphere and the atmosphere is strongly influenced by plant leaf phenology that refers to the temporal pattern of seasonal leaf onset and senescence (Arora & Boer 2005, Fisher el al. 2006). Under warming conditions, increasing greenhouse gas is expected to extend the growing season of plant leaf (Beaubien & Freeland 2000, Menzel & Fabian 1999, Chmielewski & Rötzer 2001). However, estimating leaf phenology with ecosystem models is still challenging although progress has been made in understanding the drivers of leaf phenology even at the molecular level (Sung & Amasino 2004). In the absence of process-based modeling of leaf phenology, empirical approaches in ecosystem and dynamic vegetation models have been tested with varying degrees of success (Linkosalo et al. 2008).

At regional scales, satellite-based vegetation indices have been used to characterize phenology (Asrar et al. 1989, Baret & Guyot 1991, Zhang et al. 2003, Hurley et al. 2014, Jin & Eklundh 2014, Balzarolo et al. 2016). Previous studies focusing on phenology and vegetation indices have demonstrated that spatiotemporal data from remote sensing could be used to study phenological trends (Liang et al. 2014, Yue et al. 2015). Various vegetation indices are often computed using certain combinations of remote sensing bands, such as red and infrared. For example, Moderate Resolution Imaging Spectroradiometer (MODIS) provides a product of vegetation indices at a16-day interval and a resolution of 500m, from which we could identify the shift of green-up and senescence stages of different vegetation types.

Similar to other vegetation indices, leaf area index (LAI) is a good indicator of the seasonality of vegetation cover change (Beck et al. 2006), which can be used to characterize leaf phenology changes and is closely related to the global carbon and water cycles. LAI is defined as total one-sided leaf area per unit ground surface area (Chen and Black 1992), which determines the amount of light intercepted by canopy (Chen and Cihlar 1996). It has been observed for various ecosystem types using LAI-2000, Tracing Radiation and Architecture of Canopies (TRAC) and digital hemispherical photography (DHP) in the field. Process-based models have also been used to estimate LAI directly or by combining remote sensing data (e.g., Asrar et al. 1984, Asner et al. 2003). To date, there were still significant uncertainties in estimating LAI using ecosystem models (Richardson et al. 2012).

Here we use a process-based ecosystem model, the Terrestrial Ecosystem Model (TEM; Zhuang et al. 2003, 2010), to estimate LAI. We then use the simulated LAI to examine plant leaf phenology changes. TEM is a process-based model that quantifies the dynamics of carbon, nitrogen, water, and energy at a monthly time step, using spatially-explicit data of vegetation, climate, soil and elevation (Raich et al. 1991, McGuire et al. 1992, Melillo et al. 1993, Felzer et al. 2004, Zhuang et al. 2001, 2002, 2003, 2010). TEM consists of a set of ordinary differential equations that govern the exchanges of carbon and nitrogen between soils, vegetation, and the atmosphere. However, TEM's capability to simulate LAI has not yet been evaluated with observed data. Here we take advantage of available site-level and satellite-based observation data to fully evaluate TEM. We then conduct LAI simulations for natural ecosystems in North America. The remote sensing products for the entire region and various plant function types (PFTs) are used to evaluate the model. The changes of leaf phenology are then analyzed using LAI data for North America during the period of 1985-2010. This study focuses on improving

quantification of LAI as an indicator of leaf phenology. We expect the correctly-modeled LAI and leaf phenology will improve quantification of ecosystem water, energy, and carbon dynamics.

2.3 Method

2.3.1 Overview

We first develop LAI algorithms in TEM. We then use a Markov Chain Monte Carlo (MCMC) method to acquire the best parameters at site and regional scales. Third, we verify site-level and regional LAI estimates using AmeriFlux observational data and the Advanced Very High Resolution Radiometer (AVHRR) LAI product at a spatial resolution of 0.5°×0.5°. Below, we first present our data organization at site and regional levels. Second, we describe the model development. Third, we describe the parameterization method and regional simulation protocols. Finally, we introduce how we conduct the leaf phenology change analysis by comparing model simulations and data product from remote sensing for North America from 1985 to 2010.

2.3.2 In Situ and Satellite Data

Site-level LAI observational data are collected from AmeriFlux sites (Hagen et al. 2006, Urbanski et al. 2007, Sulman et al. 2009). Six sites including Harvard Forest, University of Michigan Biological Station (UMBS), Howland Forest, Morgan Monroe State Forest, Shidler Tallgrass Prairie, and Donaldson are selected to cover major plant function types in this region (Figures 1&2). For site-level LAI calibration, we check all AmeriFlux sites that have LAI data and select the sites with continuous measurements for over 4 years with measurements for every month. We use all the measurements available for our studying period in North America from these 6 sites to optimize LAI model parameters. These six sites are the only ones that meet our data selection criteria for our study in the region. We recognize these six sites represent a limited

number of plant function types (PFT) in North America. Thus, we further calibrate the model in a spatially-explicit manner for regional LAI simulations to quantify regional LAI more accurately. The details of site and data description are documented in Table 1.

Two types of remote sensing LAI products including AVHRR and GLASS (Global LAnd Surface Satellite) are used in this study. The third-generation LAI data set from AVHRR (GIMMS LAI3g) for the period from July 1985 to December 2010 is used (Myneni et al. 1997). The AVHRR LAI product is produced using an artificial neural network method with resolution of 16km, resampled to 0.5^{o}x0.5^o degree (Claverie et al. 2016, Anav et al. 2013). The GLASS LAI algorithm (Liang et al. 2013) is based on time-series reflectance data using general regression neural networks. In general, the spatial patterns of GLASS LAI are consistent with MODIS and CYCLOPES products.

To conduct regional simulations, NCEP (National Centers for Environmental Prediction) monthly climate data in the period 1985-2010 at a spatial resolution 0.5°×0.5° including precipitation, air temperature, and cloudiness are used. In addition, data of soil texture, elevation, and plant function types (PFT) at the same spatial resolution are also used (Figure 1; Zhuang et al. 2003). AVHRR LAI product of 1985-2010 is used for regional model parameterization, while GLASS LAI is used for model evaluation.

2.3.3 Model Description

In TEM, vegetation carbon (V_c) is modeled with a differential equation:

$$\frac{dVc}{dt} = GPP - R_A - L_C \quad (1)$$

where GPP refers to gross primary production, R_A refers to autotrophic respiration and *Lc* refers to litterfall carbon. GPP is calculated as the function of maximum rate of photosynthesis carbon,

atmospheric CO_2 concentration, leaf phenology, temperature, light use and other factors (Zhuang et al. 2003). LAI is estimated based on specific leaf area (*sla*):

$$LAI(t) = sla \times l_A(t) \times leaf(t) \quad (2)$$

where *sla* is defined as the ratio of leaf area to dry leaf mass with units of $m^2g^{-1}C^{-1}$, which is one of the widely accepted leaf characteristics to study leaf traits (Wilson et al. 1999). $l_A(t)$ (g Cm^{-2}) is maximum biomass of the canopy, which is defined as a function of V_c:

$$l_A(t) = \frac{leafmxc}{1 + kleaf \times e^{COV \times V_C}} \quad (3)$$

where *leaf (t)* is a scalar, and is calculated:

$$leaf(t) = \begin{cases} minleaf, where \dfrac{Uleaf_i(t)}{Uleaf_{i-1,\max}} < minleaf \\ \dfrac{Uleaf_i(t)}{Uleaf_{i-1,\max}}, elsewhere \\ 1, where \dfrac{Uleaf_i(t)}{Uleaf_{i-1,\max}} > 1 \end{cases} \quad (4)$$

The value of *leaf (t)* resides between *minleaf* and 1, and the value in between is computed as the ratio of *Uleaf (t)* in each month to maximum *Uleaf(t)* of the previous year.

$Uleaf_i(t)$ represents the photosynthetic capacity of mature vegetation:

$$Uleaf_i(t) = aleaf \times \frac{EET}{EET_{\max}} + bleaf \times Uleaf_{i-1} + cleaf \quad (5)$$

where *aleaf*, *bleaf*, *cleaf*, and *minleaf* are coefficients for the calculation of $Uleaf_i(t)$. $Uleaf_i(t)$ is related to the estimated evapotranspiration and three parameters optimized using the data assimilation method. EET is the estimated evapotranspiration, computed from a water balance model (WBM: Vörösmarty et al. 1998). EET_{max} is the estimated maximum ET of previous year. Parameters related to LAI simulation also include *leafmxc*, *kleaf*, and *cov* (biome-specific foliage

projection cover parameter). Different plant function types have different sets of optimal parameters.

2.3.4 Model Parameterization

Site-level parameterization for LAI is conducted for different PFTs at the selected sites using observational data. At regional levels, an optimum set of parameters for each pixel is obtained using a spatially-explicit parameterization method (Chen & Zhuang 2012). Specifically, we generate optimum parameters for each 0.5° x 0.5° grid using AVHRR LAI product from 1985-1995 while the data for the period of 1995-2010 are used for model evaluation at the regional scale.

To use *in situ* and satellite data of LAI to parameterize the model, a MCMC technique is used (Metropolis et al. 1953, Hastings 1970). MCMC is a general method for simulation of stochastic processes with a specific probability density function. Specifically, a sequence of random variables is a Markov chain when the $(n+1)^{th}$ element only depends on the n^{th} element. One popular method to implement MCMC uses the Metropolis-Hasting algorithm. The basic idea of the algorithm is to generate random walk values with a proposed probability density and decide whether to accept or reject a value based on an acceptance ratio. Here we sample 10,000 parameter combinations for each site with probability *P(x)*. The algorithm is with following steps:

(i) Initialization: First choose an arbitrary $\vec{x}_0$ as the initial sample, which is the initial vector of parameters space. In the case of LAI model, $\vec{x}_0$ represents $\left(leafmxc_0, kleafc_0, sla_0, \mathrm{cov}_0, minleaf_0, aleaf_0, bleaf_0, cleaf_0\right)$. Second, choose an arbitrary Gaussian distribution $Q\left(\vec{x}_1 \mid \vec{x}_0\right)$ (centered at $\vec{x}_0$) as the proposed density (or jumping

distribution) for the sampling sequence (see Table 2 for details about initial parameter and distribution settings).

(ii) Iteration: For each time step t, generate candidate sample $\vec{x}_C$ based on $Q\left(\vec{x}_C \mid \vec{x}_t\right)$; then calculate an acceptance ratio $P\left(\vec{x}_C\right) \Big/ P\left(\vec{x}_t\right)$; if it is greater than or equals 1, accept the candidate and set $\vec{x}_{t+1} = \vec{x}_C$; if it is smaller than 1 and greater than 0, accept the candidate with a probability of the acceptance ratio. If it is not greater than 0, set $\vec{x}_{t+1} = \vec{x}_t$.

The Gaussian distribution $Q\left(\vec{x}_C \mid \vec{x}_t\right)$ is defined with a mean (the previous value for the parameter) and standard deviation (50% of the original value for the parameter) (Table 2). The best parameters for a pixel are optimized by calculating the root mean square error (RMSE) between model simulations and AVHRR LAI. GLASS LAI data are used for evaluating the model parameters by comparing with model simulations.

2.3.5 Regional Simulations and Analysis

For the regional analysis in North America, simulations are conducted for each grid with the optimized spatially-explicit parameters for the region. The regional simulated data are organized to compute regional correlations between model and satellite product. We also examine the spatial distribution of parameter values. The sensitivity analysis is done by varying parameter values in the prior parameter distribution space. Furthermore, we separate the modeling results by sub-regions including Alaska, Canada, the conterminous US and by plant function types to examine the decadal and seasonal LAI changes for different ecosystem types and areas in the region.

2.4 Results and Discussion

2.4.1 Comparison between modeled and observed leaf area index

Site-level data assimilations provide a set of optimum parameters for the six sites (Table 1 & Table 3). The parameters are evaluated with the reserved data that have not been used for parameterization. For various ecosystems, the RMSE between observed and simulated LAI is smaller than 0.8 m^2m^{-2} and correlation coefficients are greater than 0.75 (Table 4 & Figure 2). The seasonality of the observed LAI is well produced with the model. The site-level simulations are also compared well with GLASS LAI product at different sites (RMSE ranging from 0.15 to 0.78 m^2m^{-2}).

Spatially explicit parameterization shows that the parameters are with different magnitudes for each PFT (Table 5; Figure 3). Some parameters such as *kleafc* and *sla* have smaller spatial variations compared to other parameters such as *aleaf* and *bleaf.* This is because some parameters are more directly related to LAI in the model. Our previous study demonstrated that the varying parameters across space better simulated ecosystem carbon dynamics (Chen and Zhuang 2012). We thus use the derived spatially-explicit parameters based on satellite data for our regional LAI simulation.

At the regional scale, the simulated LAI for each PFT varied across space, and the simulation compares well with the satellite data for each PFT (Table 6). The TEM performs well for all representative PFTs with R^2 ranging from 0.66 to 0.80 and RMSE from 1.05 to 2.32 m^2m^{-2}. For boreal forest as a major PFT in this region, the model performs well with R^2 of 0.76 and RMSE of 1.12 m^2m^{-2}. For other seven PFTs, the model performs similarly with RMSE less than 2.4 m^2m^{-2}.

The regression between simulated and remote sensing-based monthly LAI has the slope of 1.38 and 0.84, which is close to 1, for tundra and grasslands, respectively (Figure 4). In addition,

satellite-based LAI is saturated at 6 m^2m^{-2}, while TEM modeled LAI has more reasonable values. In general, the model performs well for tundra, boreal forest, temperate coniferous/deciduous forest, grasslands and xeric shrublands, slightly deteriorates for temperate deciduous forests (RMSE=2.32 m^2m^{-2}) (Table 6). Using the spatially explicit parameters, the TEM better simulates LAI compared to using a single set of parameters for each PFT in the region. The correlation analysis suggests that monthly LAI is highly correlated with temperature (R^2=0.76) and precipitation (R^2=0.46) in North America. Temperature plays a more significant role in LAI changes (Table 7).

To determine the distribution of LAI changes in North America, three sub-regions including Alaska, Canada and the conterminous US are analyzed (Figure 5). In Alaska, monthly LAI did not change significantly with an increase of 0.02 m^2m^{-2} from 2001 to 2010 compared with that in 1981-1990. The highest monthly average is in September, from 1.68 to 1.86 m^2m^{-2}. In Canada, monthly average LAI increased by 0.015 m^2m^{-2} and RMSE less than 0.1 m^2m^{-2}. In the conterminous US, there was the largest increase by 0.06 m^2m^{-2}, with an ineligible increase (>0.1 m^2m^{-2}) from September to December. The conterminous US contributes the most to the average LAI increase in North America during the three-decade study period. The modeled LAI fits best with satellite-based LAI product in the conterminous US (R^2=0.81, slope =0.78), while model also captures the satellite-based LAI for Alaska and Canada (Figure 5).

Different sub-regions show various correlations with climate. In Canada, monthly LAI has higher correlations (R^2=0.78) with air temperature than in the conterminous US (R^2=0.68), while lower correlations with precipitation (R^2=0.30) than in the conterminous US (R^2=0.58). Leaf phenology in higher latitude regions are more affected by temperature and less by precipitation (Table 8).

From 1985 to 2010, temperate coniferous and temperate deciduous LAI increased by 0.03 and 0.06 m^2m^{-2}, respectively. The increase of monthly LAI of deciduous forests is mostly due to increased monthly mean temperature. Overall, TEM captures the maximum and minimum monthly LAI for wet tundra, boreal forests, temperate coniferous forests, temperate deciduous forests, grasslands and xeric shrublands, with RMSE less than 0.5 m^2m^{-2}. Average monthly LAI shows different trends for different PFTs (Figure 4). We further separated the conterminous US into 4 sub-regions including southwest (California, Nevada, Utah, Colorado, Arizona, New Mexico, Oklahoma, and Texas), southeast (Arkansas, Louisiana, Mississippi, Alabama, Georgia, Florida, South Carolina, Tennessee, North Carolina, Kentucky, Virginia, and West Virginia), northwest (Washington, Oregon, Idaho, Montana, Wyoming), and northeast (Maine, New Hampshire, Vermont, Massachusetts, Rhode Island, Connecticut, New York, New Jersey, and Pennsylvania). TEM performs similarly for these sub-regions with R^2 ranging from 0.65 to 0.86. In the northwest, the model performs the best (R^2 = 0.86) (Figure 6).

2.4.2 Phenology change analysis

Our modeled LAI results indicate that there was a phenology trend of earlier spring and later autumn, which have been reported in several previous studies (Myneni et al. 1997, Barichivich et al. 2013, Keenan et al. 2014). Modeled monthly LAI in April and September all increased between two decades from 1981-1990 to 2001-2010 at 0.03 m^2m^{-2} for April and 0.24 m^2m^{-2} for September, respectively (Figure 7). There was an increase of LAI at 0.3 m^2m^{-2} between the 1980s and 2000s in majority area of North America. The exception occurs mostly at high latitudes or lands covered with vegetation that typically has low LAI. Similarly, AVHRR LAI data product also indicated that there was an increase of monthly LAI in April and September from the 1980s

to1990s, especially in the conterminous US, demonstrating phenology changed with an earlier leaf start and later leaf fall. Analysis for each PFT shows temperate deciduous forests had the most obvious change. Our temporal regression between LAI in April and September and time shows positive correlations for April (R^2 = 0.72) and September (R^2 = 0.64), respectively, suggesting there are significant increases of April and September LAI over the period.

In general, the region had an earlier greening trend from March to June, primarily due to temperature increasing during the study period (Figure 5). April LAI increased more in the conterminous US (0.04 m^2m^{-2}) compared to Alaska (0.003 m^2m^{-2}) and Canada (0.001 m^2m^{-2}). Similarly, the increase of LAI also occurred in September in Alaska (0.05 m^2m^{-2}), Canada (0.04 m^2m^{-2}), and the conterminous US (0.27 m^2m^{-2}).

Compared with other recent studies focused on phenology in North America using remote sensing data (Melaas et al. 2016, Richardson et al. 2012), our simulations showed similar patterns of earlier spring onset and longer growing season in the region. However, the shift of the end of growing season is harder to capture than the start of growing season in our simulations.

Greening feature characterized as increasing LAI varied among different PFTs (Figure 7). Temperate deciduous forests had a larger increase than other PFTs, with 0.07 m^2m^{-2} in April and 0.31 m^2m^{-2} in September. Boreal forests, accounting for 30% grids in North America had an increase of 0.04 m^2m^{-2} in April and 0.27 m^2m^{-2} in September, respectively. Previous studies have demonstrated the response of vegetation phenology to warming climate in a similar way (e.g., Zhang et al. 2007). In addition to the increased LAI magnitude, it is widely acknowledged that the timing of phenological events including start and end of growing season is sensitive to climate change in various regions (Chuine et al. 2004, Liu et al. 2016). Our analysis indicates that the timing of the leaf start and leaf fall is significantly and positively correlated ($R^2 > 0.5$, *p-value* <

0.01) between modeled LAI in April and September (Figure 8), suggesting that the growing season length has increased in the last few decades in North America, which is consistent with recent studies (Myneni et al. 1997, Keenan et al. 2014).

Our LAI and phenology analysis is limited by the availability of quality observation data of LAI. LAI data are often only available for growing season at observational sites. Thus, the parameters are not well constrained for capturing the LAI seasonality. Our uncertainty analysis by varying parameters of LAI within the prior probability distribution indicates that the simulated monthly regional LAI varies by 36% (Figure 9). For the study period, the increase of regional LAI is (3±0.5)% due to uncertain parameters. In addition, LAI is modeled as a function of vegetation carbon with a few parameters, which does not sufficiently represent the processes determining LAI. Future improvement shall include more biological processes related to leaf phenology.

2.4.3 Future applications of LAI modeling

Our next steps include integrating the improved LAI modeling into GPP and evapotranspiration (ET) quantification with TEM. In previous studies of carbon dynamics with TEM (e.g., Zhu et al. 2013), LAI was not used for modeling GPP. With our spatial-explicitly calibrated LAI, we now could improve GPP simulations, thus net primary production (NPP) and net ecosystem production defined as the difference of NPP and heterotrophic respiration. We will also be able to integrate LAI into ET quantification with TEM. Previously we have used the Penman-Monteith equation to estimate ET by using satellite-based or observed LAI with TEM (e.g., Liu et al. 2013). With improved LAI modeling, we could improve the quantification of ET using TEM for certain time periods and spatial areas of interest that are not limited within

satellite-based LAI periods and regions, such as for the 21st century and the whole North America. The improved LAI modeling within terrestrial ecosystem models could also be an important component in earth system models to quantify feedbacks between terrestrial biosphere and the climate.

2.5 Conclusions

This study improves LAI algorithms within a process-based biogeochemistry model to study phenology patterns in North America. Observational LAI data from AmeriFlux network is used to optimize parameters. Remote sensing data of AVHRR LAI product is used to optimize parameters at regional scales. Comparison between model simulations and satellite-based LAI for the region shows that the model is able to estimate the seasonality and interannual variability of LAI in the region. The average LAI in recent three decades has increased by 3% on average in the region. The simulated monthly average LAI increase during study period was 1.24, 1.46 and 2.21 m^2m^{-2}, in Alaska, Canada and the conterminous US, respectively, which is consistent with satellite observations. In comparison with satellite data, the model captured the phenology change for key plant functional types from 1985 to 2010. The model also performed well to capture the regional phenology change in Alaska, Canada, and the conterminous US. This study provides a way to estimate the changes of leaf area index and phenology, which will improve future carbon and water cycling quantification for the region.

2.6 Acknowledgement

This research was supported by a NSF project (#1028291) funded to Q.Z. We acknowledge the computing support from the Rosen Center for Advanced Computing at Purdue. We also

acknowledge that the AmeriFlux network provides multiple LAI and other auxiliary datasets for this model-data fusion study.

Table 2.1 Description of AmeriFlux sites with observed LAI for site-level data assimilation

Site Name /FLUXNET ID	Longitude (degree)	Latitude (degree)	Plant Function Type	Data Period	Reference
Harvard Forest / US-Ha1	-72.17	42.54	Deciduous broadleaf forest	2005-2008	Urbanski et al. 2004, van Gorsel et al. 2009
UMBS / US-UMB	-84.71	45.56	Deciduous broadleaf forest	1999-2007	Curtis et al. 2002, Schmid et al. 2003
Howland Forest /US-Ho1	-68.74	45.2	Evergreen needleleaf forest	2006	Hagen et al. 2006, Richardson et al. 2006
Morgan Monroe State Forest / US-MMS	-86.41	39.32	Deciduous broadleaf forest	1999-2006	Richardson et al. 2012, Oliphant et al. 2011
Shidler Tallgrass Prairie / US-Shd	-96.68	36.93	Grasslands	1997-2000	Schmidt et al. 2011, Schwalm et al. 2010
Donaldson / US-SP3	-82.16	29.75	Evergreen needleleaf forest	1999-2007	Bracho et al. 2012, Thompson et al. 2011

Table 2.2 Prior values of parameters related to LAI estimation

Acronym	Definition	Units	Mean	Standard Deviation
leafmxc	Maximum biomass of the canopy	gCm^{-2}	500	250
kleafc	Biome-specific allocation parameter	None	2	1
sla	Specific leaf area	$m^2(gC)^{-1}$	0.008	0.004
cov	Biome-specific foliage projection cover parameter	None	-0.005	-0.0025
minleaf	Minimum photosynthesis capacity	None	0.5	0.25
aleaf	Coefficient A to model relative photosynthetic capacity of vegetation	None	0.5	0.25
bleaf	Coefficient B to model relative photosynthetic capacity of vegetation	None	0.5	0.25
cleaf	Coefficient C to model relative photosynthetic capacity of vegetation	None	0	0.5

Table 2.3 Best parameters for LAI modeling at calibration sites

Site	Harvard Forest	UMBS	Howland Forest	Morgan Monroe State Fores	Shidler Tallgrass Prairie	Donaldson
leafmxc	653.586	579.135	634.889	702.178	585.261	590.308
kleafc	1.775	2.172	2.225	2.825	2.113	1.902
sla	0.0094	0.0066	0.0099	0.0071	0.0114	0.0103
cov	-0.000521	-0.001031	-0.000616	-0.000329	-0.00031	-0.0006
minleaf	0.367	0.375	0.542	0.194	0.128	0.49
aleaf	0.797	0.343	0.181	0.239	0.592	0.224
bleaf	0.527	0.487	0.674	0.463	0.434	0.649
cleaf	0.135	0.13	0.374	0.0195	-0.115	0.102

Table 2.4 Model-data fitting statistics of site-level LAI between model simulations and observations

Site	Correlation Coefficient	Slope	Intercept (m^2m^{-2})	RMSE (m^2m^{-2})
Harvard Forest	0.96	0.93	0.50	0.49
UMBS	0.87	0.78	0.57	0.40
Howland Forest	0.96	0.82	0.97	0.15
Morgan Monroe State Forest	0.85	0.73	0.76	0.78
Shidler Tallgrass Prairie	0.82	0.67	0.33	0.49
Donaldson	0.75	0.59	2.06	0.67

Table 2.5 Optimal parameters from regional assimilation organized by plant function type from 1985 to 2010

Type	Leafmxc	kleafc	sla	cov	minleaf	aleaf	bleaf	cleaf
Alpine Tundra & Polar Desert	642±240	1.66±0.16	0.010±0.003	-0.0006±0.0045	0.11±0.17	0.60±0.15	0.39±0.07	0.10±0.04
Wet Tundra	442±235	1.67±0.14	0.008±0.002	-0.0004±0.0011	0.22±0.19	0.53±0.17	0.38±0.07	0.11±0.06
Boreal Forest	578±203	1.68±0.42	0.008±0.001	-0.0013±0.0097	0.08±0.13	0.50±0.13	0.37±0.05	0.12±0.02
Temperate Coniferous Forest	714±154	1.76±0.82	0.009±0.002	-0.0115±0.0315	0.27±0.22	0.38±0.15	0.38±0.11	0.12±0.06
Temperate Deciduous Forest	649±155	1.66±0.89	0.008±0.001	-0.0373±0.0482	0.12±0.18	0.52±0.19	0.35±0.09	0.11±0.04
Grassland	575±208	1.66±0.13	0.010±0.003	-0.0003±0.0000	0.23±0.21	0.50±0.20	0.37±0.11	0.11±0.05
Xeric Shrubland	399±227	1.67±0.13	0.008±0.001	-0.0003±0.0002	0.40±0.18	0.43±0.19	0.40±0.15	0.13±0.08
Tropical Forest	615±197	2.09±1.18	0.008±0.001	-0.0332±0.0468	0.45±0.15	0.34±0.21	0.48±0.18	0.09±0.14

Table 2.6 Fitting statistics of regional LAI simulations and satellite data

Plant Function Type	Number of simulation grids	R^2	RMSE (m^2m^{-2})
Alpine tundra & polar desert	510	0.71	2.25
Wet tundra	1432	0.76	1.05
Boreal forest	3613	0.76	1.12
Temperate coniferous forests	1496	0.66	1.15
Temperate deciduous forests	449	0.67	1.32
Grasslands	1541	0.76	1.35
Xeric shrublands	725	0.69	1.27
Tropical forests	345	0.80	2.13

Table 2.7 Correlation between forcing data and modeled LAI. Column (a) shows correlation between LAI and temperature; column (b) shows correlation between LAI and precipitation

Site	(a)	(b)
Harvard Forest	0.75	0.48
UMBS	0.72	0.52
Howland Forest	0.65	0.42
Morgan Monroe State Forest	0.68	0.45
Shidler Tallgrass Prairie	0.52	0.39
Donaldson	0.55	0.41

Table 2.8 Correlation between forcing data and LAI simulation for each sub-region. Column (a) shows correlation between LAI and temperature; column (b) shows correlation between LAI and precipitation

Sub-region in North America	(a)	(b)
Alaska	0.56	0.43
Canada	0.78	0.3
Conterminous US	0.68	0.58

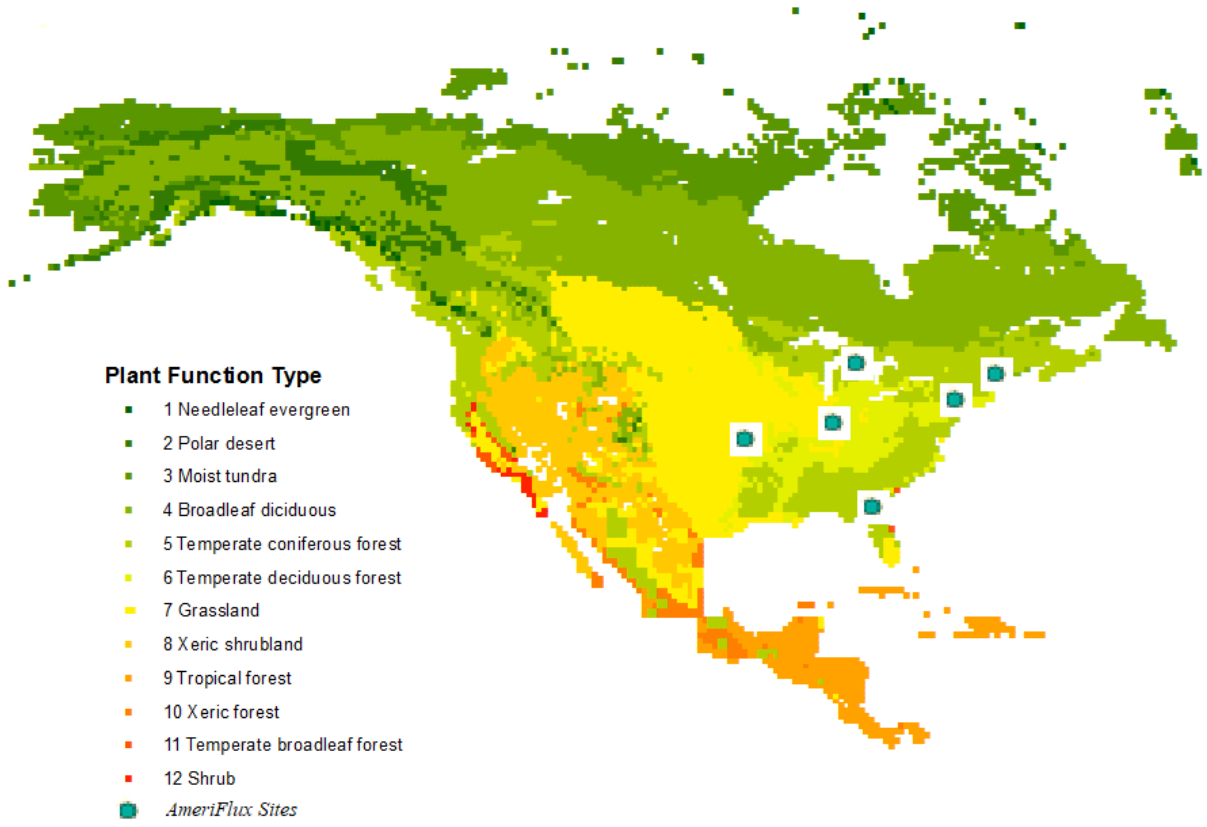

Figure 2.1 Plant function type (PFT) distribution in North America (Zhuang et al., 2003). AmeriFlux sites used for model calibration is also displayed.

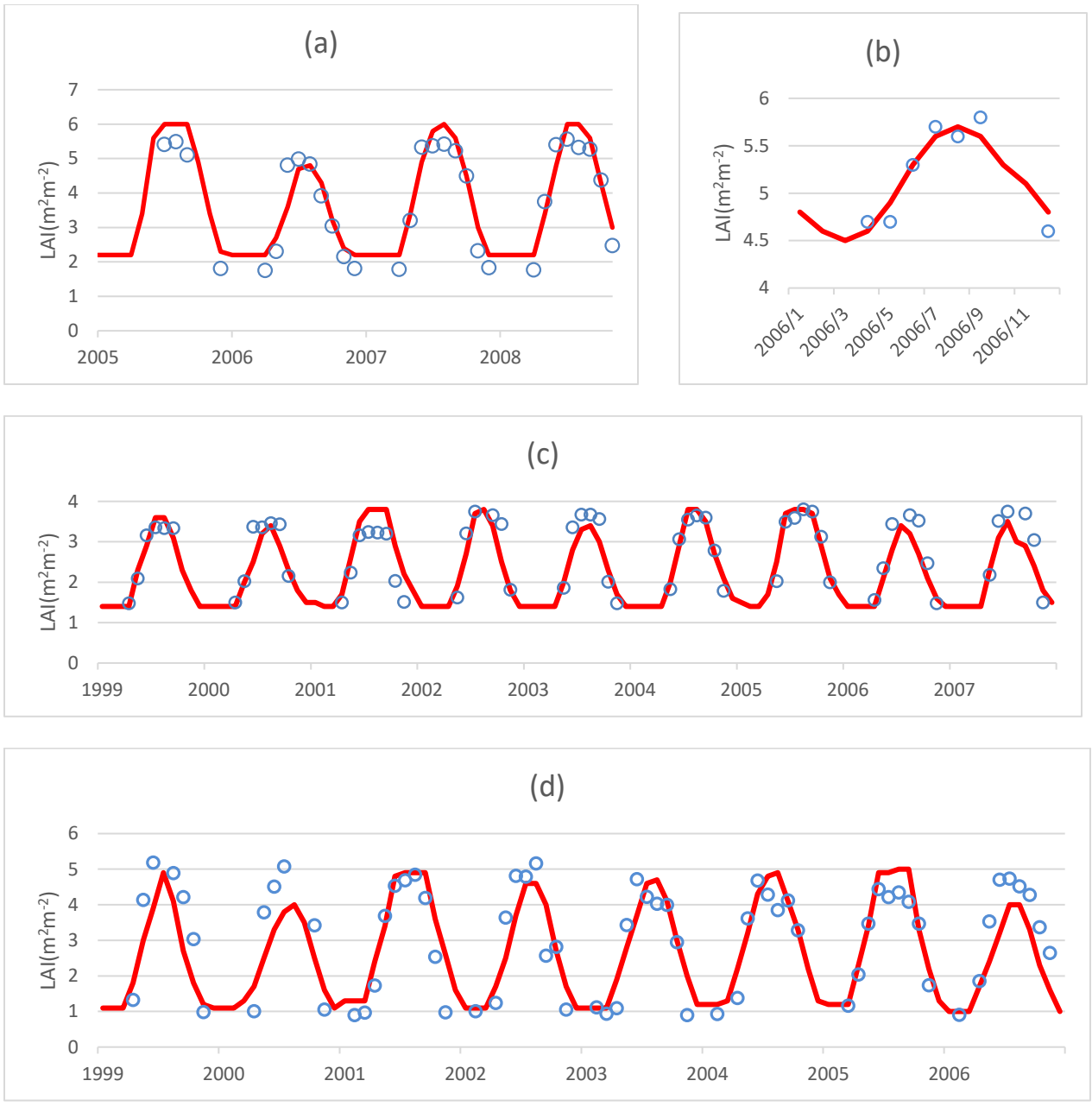

Figure 2.2 TEM simulated LAI (m2m-2) by applying the optimal parameters and in situ observational data, data assimilation is conducted for sites (a) Harvard Forest, (b) Howland forest, (c) University of Michigan Biological Station (UMBS), (d) Morgan Monroe State F

Figure 2.2 Continued

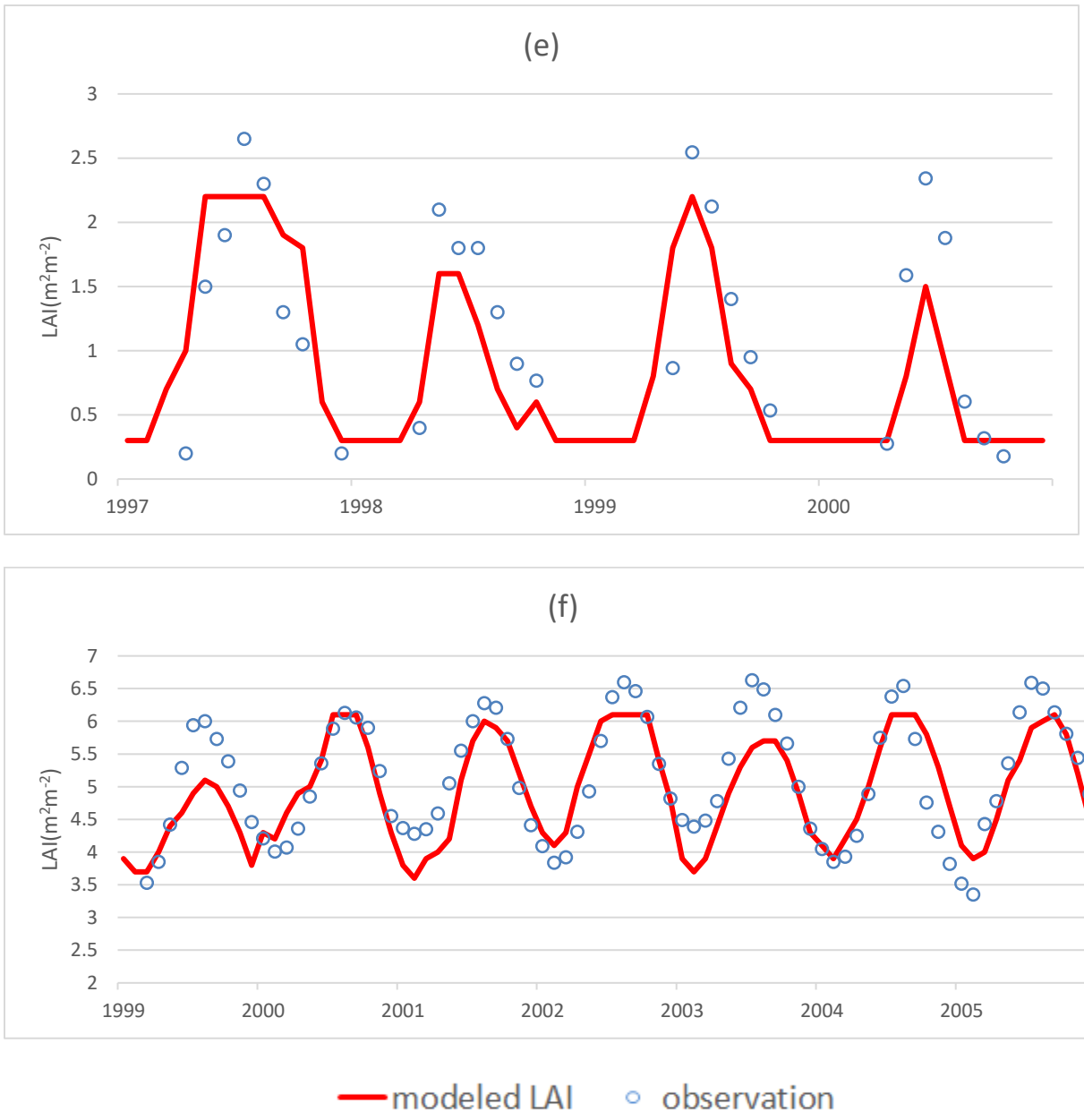

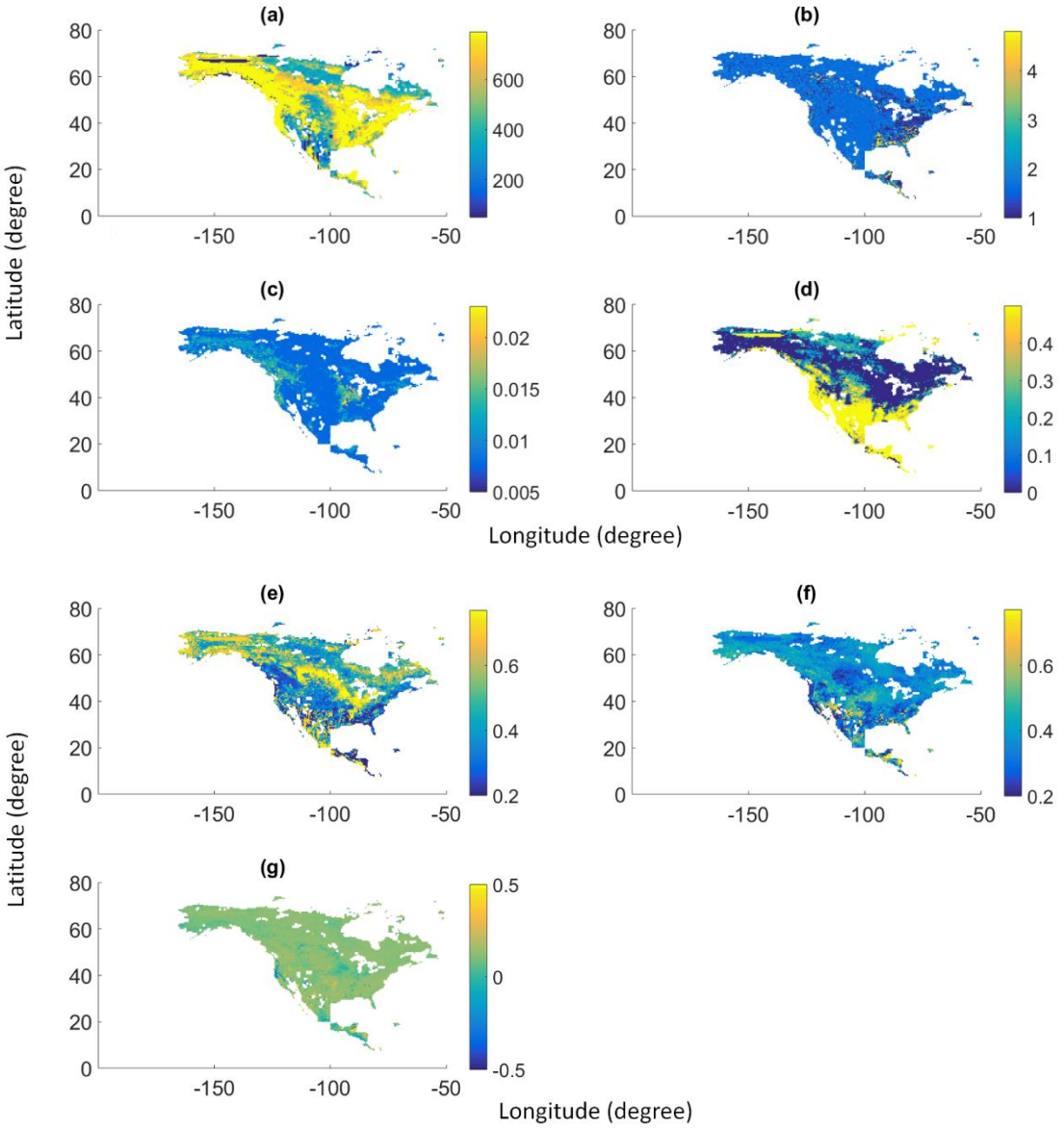

Figure 2.3 Distribution of optimum parameters for spatially explicit regional simulations: (a) leafmxc (gCm-2), (b) kleaf, (c) sla (m2(gc)-1), (d) minleaf (unitless), (e) aleaf (unitless), (f) bleaf (unitless), (g) cleaf (unitless)

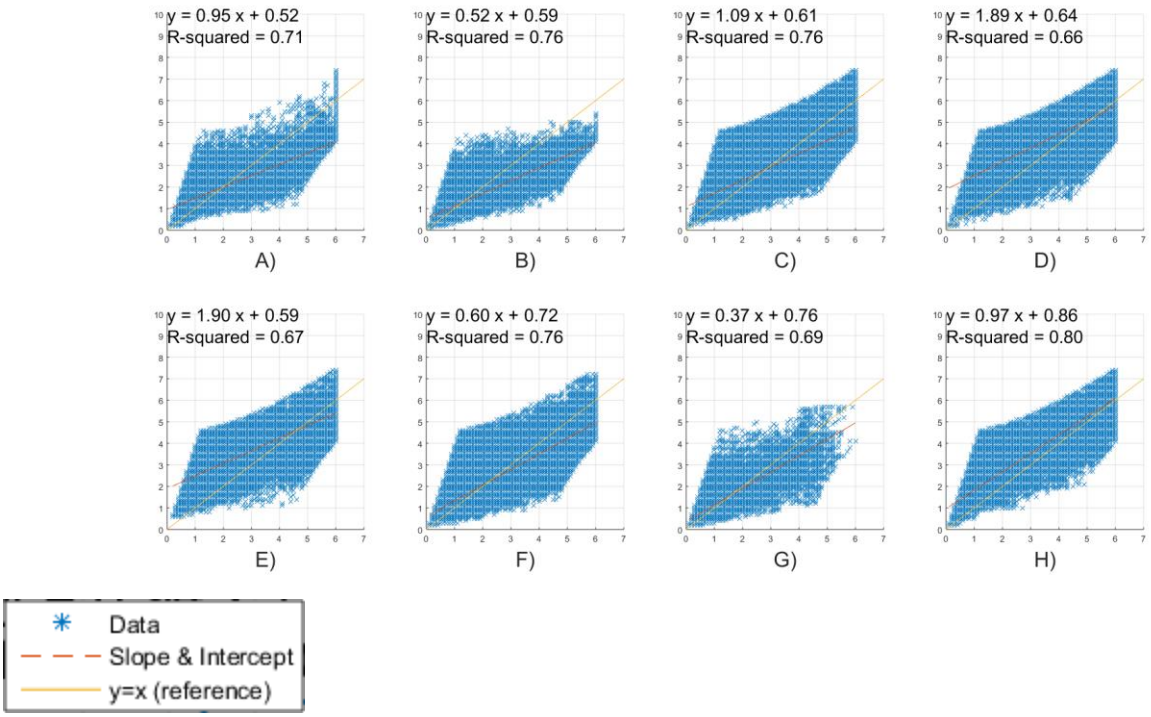

Figure 2.4 Comparison between simulated monthly LAI (m2m-2) and remote sensing (AVHRR) LAI product of North America categorized by plant function type: A) Alpine tundra and polar desert; B) Wet Tundra; C) Boreal forest; D) Temperate coniferous forests; E) Temperate

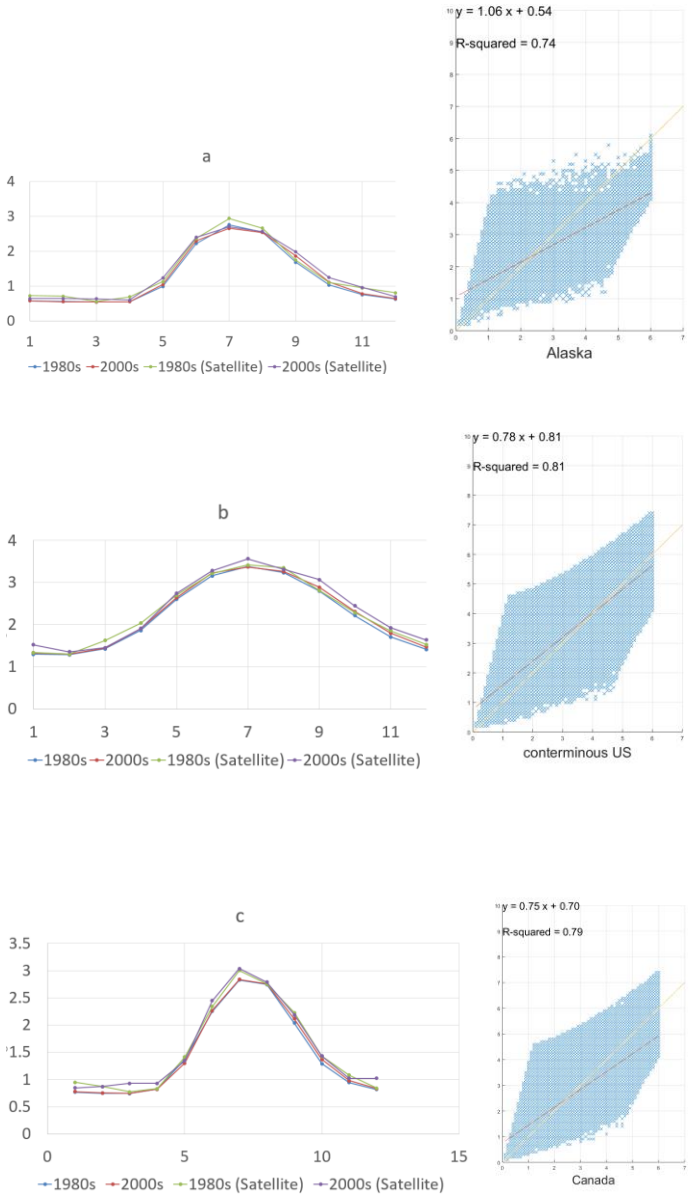

Figure 2.5 Comparison between modeled and satellite-based monthly average LAI for 3 sub-regions in North America: a) Alaska; b) Conterminous US; c) Canada. Y-axis is simulated and X-axis is satellite data.

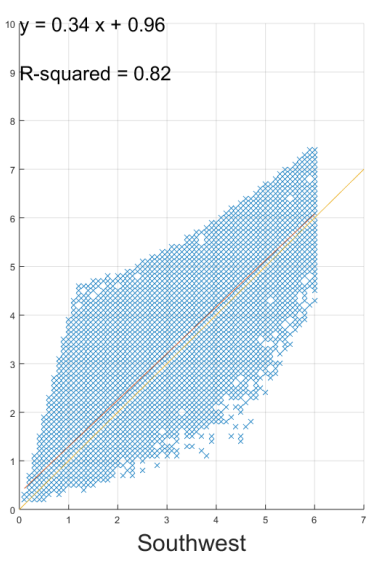

a)

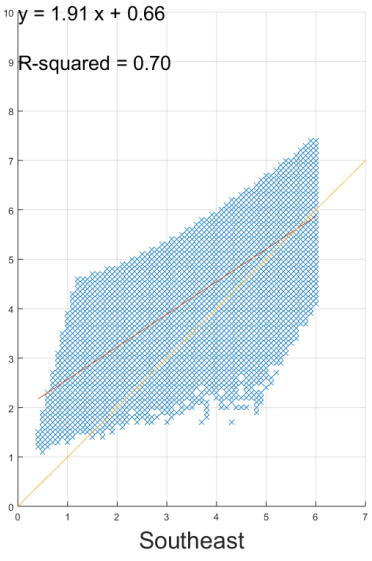

b)

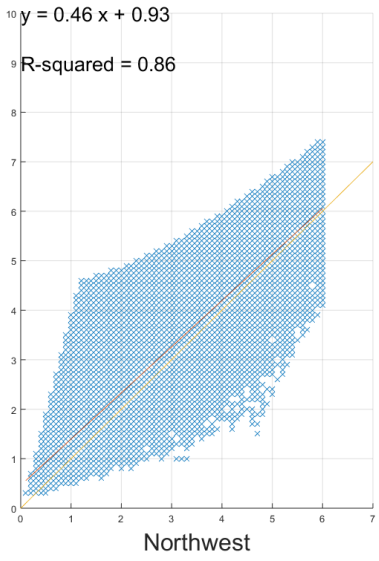

c)

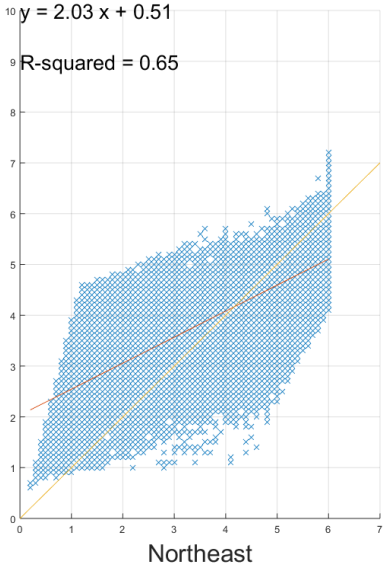

d)

Figure 2.6 Comparison between modeled (Y-axis) and satellite-based (X-axis) monthly average LAI for 4 sub-regions in the Conterminous US: a) Southwest; b) Southeast; c) Northwest, d) Northeast

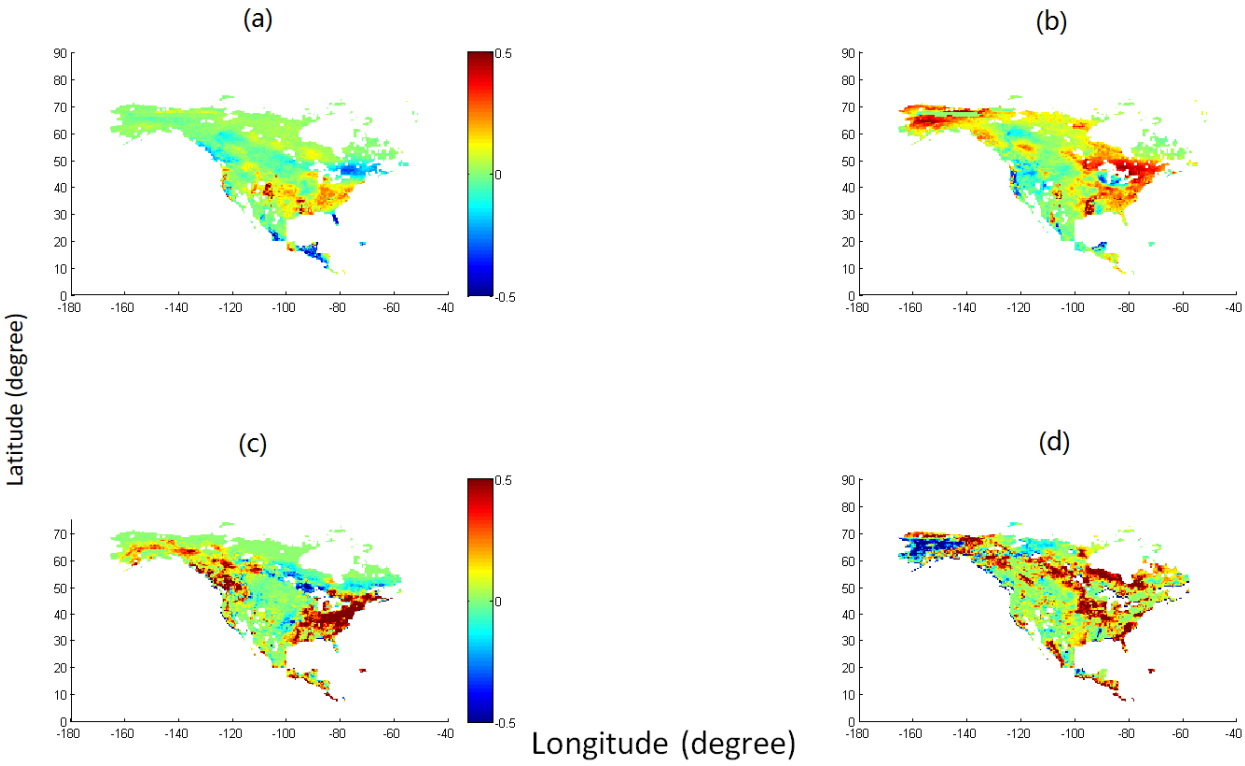

Figure 2.7 Average monthly TEM-modeled LAI increase in April (a) and September (b) from1981-1990 to 2001-2010; Average monthly AVHRR LAI increase in April (c) and September (d) from 1985-1990 to 1991-2000

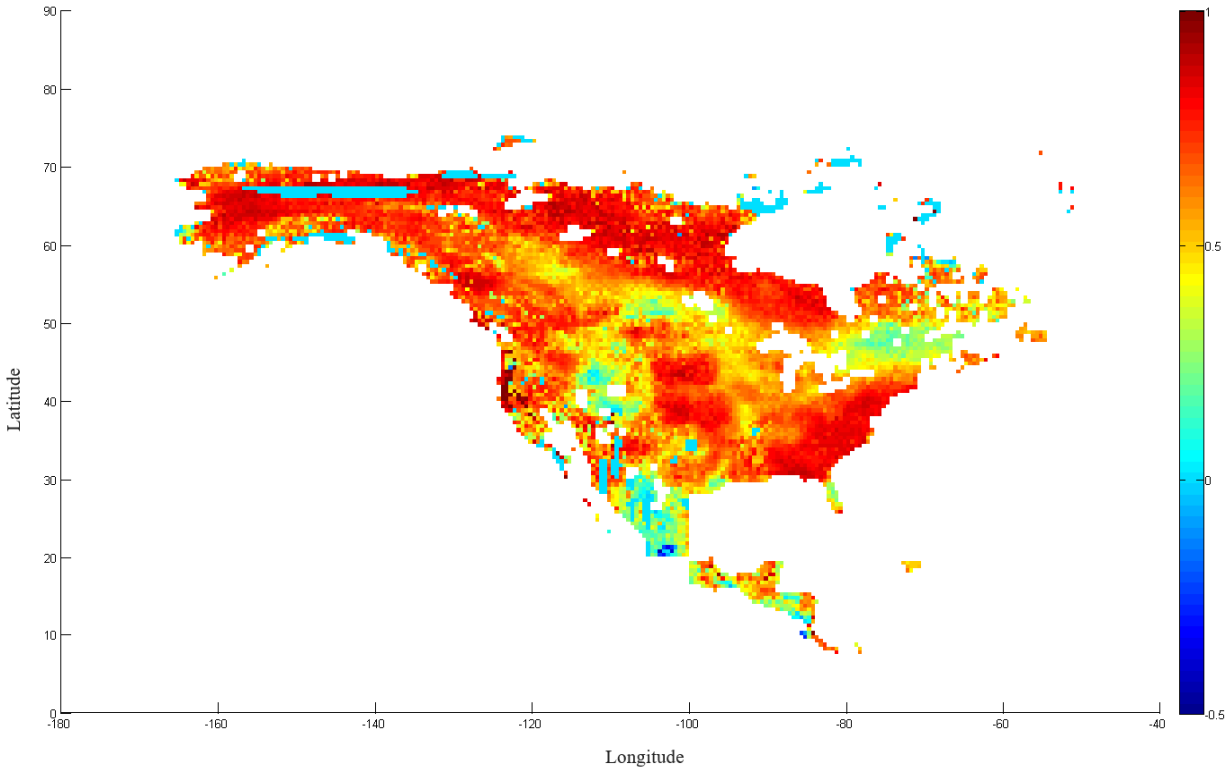

Figure 2.8 Correlation Coefficients between TEM simulated LAI in April and September from 1985 to 2010

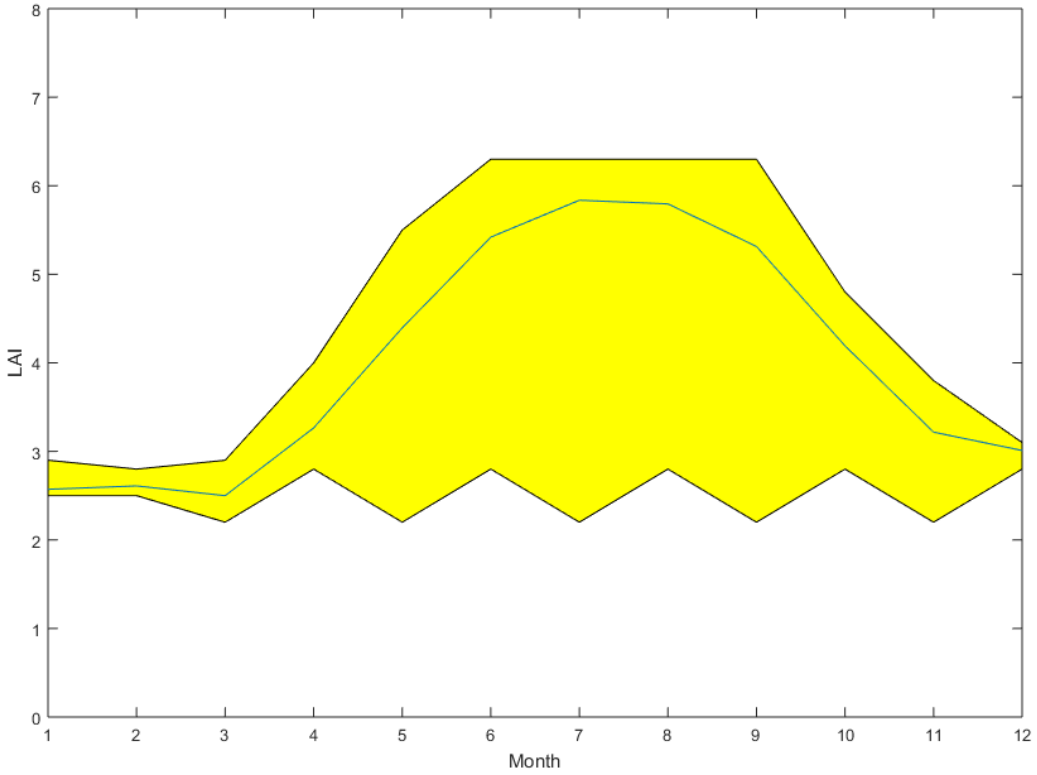

Figure 2.9 Uncertainty analysis of modeled regional LAI by varying parameters between 1985 and 2010: upper bound, lower bound, and mean month LAI values.

CHAPTER 3. RESPONSES OF EVAPOTRANSPIRATION TO CLIMATE CHANGE IN NORTH AMERICA: IMPLICATIONS TO WATER RESOURCE AND THE CLIMATE SYSTEM

3.1 Abstract

Accurate quantification of evapotranspiration (ET) is important to understanding its role in the global hydrological cycle of terrestrial ecosystems and feedbacks to the climate system. This study improves ET quantification in North America using a data assimilation technique and a process-based terrestrial ecosystem model as well as in situ and satellite data. ET is modeled using the Penman-Monteith equation with an improved leaf area index (LAI) algorithm in a biogeochemistry model, the Terrestrial Ecosystem Model (TEM). The evaluated TEM was used to estimate ET at site and regional scales in North America from 2000 to 2010. The estimated annual ET varies from 420 to 450 mm·yr-1 with the improved model, close to MODIS monthly data with root-mean-square-error less than 10 mm·month-1 for the study period. Alaska, Canada, and the conterminous US accounts for 33%, 6% and 61% of the regional ET, respectively. Water availability, the difference between precipitation and ET, is 181mm month-1, averaged from 2000 to 2010. Under IPCC RCP 2.6 and RCP 8.5 scenarios, the regional ET increases by 11% and 24%, respectively. Consequently, the water availability decreases in the region by 2.4% and 23.7%, respectively. For the period of 2020-2100, due to uncertain parameters, TEM versions integrated with three different ET algorithms estimated the regional ET in the US are 430.5±10.5 mm·yr-1, 482.1±11.2 mm·yr-1, 489.7±13.4 mm·yr-1, and the available water is -105.3±8.7 mm·yr-1, -20.3±11.9 mm·yr-1, -126.2±15.4 mm·yr-1, respectively, by the end of the 21st century. Our analysis indicates that the North America will get drier under future climate conditions, which will impact the regional water resource and the climate system.

3.2 Introduction

Evapotranspiration (ET) is an important water flux in the terrestrial ecosystem hydrological cycle (Dolman & De Jeu, 2010) and is also a key energy flux of the land surface. ET links the atmosphere and ecosphere through the energy exchange and biogeochemical cycles (Betts et al., 1996; Mu et al., 2007; Sun et al., 2011; Katul et al., 2012). Different models showed that 60~67% of annual precipitation returns as ET to the atmosphere (Vörösmarty et al., 1998; Miralles et al., 2011; Zhang et al., 2016). The response of ET to increasing temperature and greenhouse gas concentrations will impact the climate system and water availability to human system. Accurate quantification of ET is important to estimating regional water balance and water availability, an important ecosystem service (Mooney et al., 2005) and conducting economic analysis (Vörösmarty et al., 2010).

To adequately quantify regional ET across space and time, terrestrial ecosystem models with well-constrained parameters using observed data are needed. Currently, ET quantification is still of large uncertainties due to uncertain forcing data and inadequate representation of the physical processes in the models (Liu et al., 2015). The uncertainties come from different environmental factors including plant phenology, soil moisture, solar radiation, temperature and wind speed. Previous quantification of ET in North America suffered from using a limited amount of *in situ* data of ET for model parameterization and verification (Liu et al., 2014). In recent decades, satellite and remote sensing have provided continuous ET data at both high spatial and temporal resolutions at the global scale (Allen et al., 2005). For instance, MODIS ET (Mu et al., 2007) is available from 2000 to 2010 at spatial resolution of 1 km and 8-day time resolution. This product was estimated using the improved ET algorithm (Mu et al., 2011) based on Penman-Monteith equation (Monteith, 1965). Global Potential Evapo-Transpiration (Global-

PET) dataset (Zomer et al., 2008) is another high-resolution (30 arc seconds, about 1 km at equator) global dataset, which was developed by combining four different algorithms including FAO application, Thornthwaite (1948), Thornthwaite modified by Holland (1978), and Hargreaves et al. (1985). Different methods of calculating ET have been tested for different regions (Liu et al., 2014; Lu et al., 2010).

Plant transpiration (T), an important component of ET, is highly dependent on plant phenology, an indicator of seasonal variations of ecosystems (Edwards & Richardson, 2004). Plant phenology as a periodical feature of global vegetation dynamics can be studied using vegetation index (Zhang et al., 2013). The timing of start and end of vegetation growing is an important depiction of phenology. Therefore, satellite-based vegetation index (VI) has been used to characterize phenology (Asrar et al., 1989; Baret & Guyot, 1991). Leaf Area Index (LAI) as a VI is important to modeling evapotranspiration (ET) and photosynthesis (Duchemin, 2006; Wiegand et al., 1979). For instance, the Penman-Monteith ET is modeled as a function of LAI (Allen, 2000).

Some studies have used simple approaches to estimate ET, such as by linking ET and remote sensing indices directly (Sobrino et al., 2005; Wang et al., 2007), and using empirical functions to up-scale site measurements to a region (Hargreaves et al., 2003). The uncertainties from these existing studies are still large.

North America is a critical region for Earth's climate (Rasmusson et al., 1968; Biederman et al., 2016). The region is sensitive to climate change and feedbacks significantly to the global climate system (IPCC, 2014). It extends within 10° of latitude of both the equator and the North Pole and embraces every climatic zone from tropical rain forest and savanna on the lowlands of the Central America to areas of permanent ice cap in central Greenland. Subarctic and tundra

climates prevail in north Canada and Alaska, and desert and semiarid conditions are found in interior regions cut off by high mountains from rain-bearing westerly winds. A large proportion of the continent has temperate climates, which are very favorable to settlement and agriculture.

Previous studies focusing on evapotranspiration in North America have indicated that ET is sensitive to surface (e.g., plant canopy) conductance (Wilson et al., 2000). Therefore, this study integrates our well-calibrated leaf area index (LAI) model (Qu and Zhuang, 2017) into the Terrestrial Ecosystem Model (TEM; Zhuang et al., 2003, 2010) to quantify ET in North America. This study also takes advantage of the existing ET data to verify TEM simulations of ET before applying the model to the region. We revise ET algorithms in TEM to estimate monthly ET and water availability, defined as the difference between precipitation and ET. We expect the revised ET improves the water balance model (WBM; Vörösmarty et al., 1998) to estimate soil moisture. To test this, high-resolution soil moisture satellite data of SMAP (NASA Soil Moisture Active Passive) are used to evaluate the model. In addition, three different algorithms of ET estimates are also adopted into TEM and evaluated. The revised TEM is finally used to investigate the ET response to climate change from 2000 to 2010 and in the 21st century for the North America. Water availability for the historical period and the 21st century is further evaluated in the context of water availability to the region and climatic impacts.

3.3 Method

3.3.1 Data

To quantify ET in North America, NCEP (National Centers for Environmental Prediction) global monthly climate data for the period 1985-2010 at a spatial resolution of 0.5°×0.5° including precipitation, air temperature, and cloudiness are used. In addition, data of soil texture, elevation, and plant function types (PFT) at the same spatial resolution are also used (Zhuang et al., 2003). MODIS monthly ET product from 2000 to 2010 at a spatial resolution $0.5^o \times 0.5^o$ is used to verify ET model (Mu et al., 2007). To evaluate the revised TEM performance in estimating soil moisture, high-resolution soil moisture satellite data of SMAP (NASA Soil Moisture Active Passive) provided by Alaska Satellite Facility (ASF) and National Snow and Ice Data Center (NSIDC) is used. Specifically, the level-4 soil moisture data at soil surface and root zone at a 9-km resolution and every 7-day time step are used.

Future climate scenarios from 2016 to 2100 were generated under representative concentration pathways (RCPs), within Coupled Model Inter-Comparison Project phase 5 (CMIP5). A total of 6 scenarios simulation are combined as multi-mean value as forcing data for TEM to do simulation in the 21st century. Here we use the RCP 2.6 (Van Vuureen et al., 2007) and RCP 8.5 (Riahi et al., 2007) as two extreme case scenarios to examine changes in ET and water availability during the 21st century.

3.3.2 Model Modification

Previous simulation of ET with TEM is based on the following formulae of potential evapotranspiration (PET) (Jensen & Haise, 1963):

$$PET = \left[\left(0.014 \times \left(1.8 \times T\right) + 32\right) - 0.37\right] \times R_S \times 0.016742 \times MD \qquad (1)$$

Where T is monthly average air temperature (℃), R_S is the mean monthly short-wave radiation on top of the canopy (Cal cm^{-2} d^{-1}) calculated in TEM based on latitude, date and cloudiness (Pan et al., 1996). MD is the number of days per month. This PET algorithm lacks the consideration of net outgoing long-wave radiation, and the aerodynamic aspects of ET on the atmospheric demand for water vapor. Therefore, PET estimated from the equation tends to underestimate ET in the spring and overestimate in the summer.

In this study, we revised the actual ET algorithm by integrating the effects of leaf area index (LAI) into Penman-Monteith (P-M) equation (Monteith, 1965; Allen et al., 1998) in addition to considering the effects of radiation and temperature effects:

$$\lambda ET = \frac{\Delta \cdot (R_n - G) + \rho_a \cdot c_p \cdot \frac{(e_s - e_a)}{r_a}}{\Delta + \gamma \cdot \left(1 + \frac{r_s}{r_a}\right)} \quad \text{..... (2)}$$

Where r_s represents the surface resistance ($s \cdot m^{-1}$), which is closely related to LAI, which is modeled in Qu and Zhuang (2018); r_a is aerodynamic resistance ($s \cdot m^{-1}$). Δ is the derivative of the saturation water vapor to temperature. $R_n - G$ is the available energy, $e_s - e_a$ is the water vapor pressure deficit (VPD). r_s is calculated as:

$$r_s = \frac{r_i}{LAI_{active}} \quad \text{..... (3)}$$

where r_i is bulk stomatal resistance of the well-illuminated leaf. LAI_{active} is the active leaf area index (here we use half of improved LAI to represent), which reflects the ratio of sunlit leaf area to the soil surface. For other parameters, we use equations (7) - (10):

$$r_a = \frac{208}{u_2} \quad \text{.....(4)}$$

where u_2 is the wind speed at height of 2 meters.

Atmospheric pressure, $P = 101.3 \times \left(\frac{293 - 0.0065z}{293} \right)^{5.26}$ …….(5)

where z is elevation (m).

Saturated water vapor pressure, $e_s = 0.6108 e^{\left(\frac{17.27T}{T+237.3} \right)}$ ……(6)

where T is temperature in degree Celsius.

The slope of vapor pressure: $\Delta = \frac{4098 \left[0.6108 e^{\frac{17.27T}{T+237.3}} \right]}{\left(T + 237.3 \right)^2}$

…….....(7)

To compute net radiation in each grid cell, equations (8) -(11) are used:

$R_n = R_{ns} - R_{nl}$ …… (8)

where R_{ns} is net shortwave radiation (W m^{-2}), R_{nl} is net longwave radiation (W m^{-2}).

The solar radiation is: $R_s = \left(a_s + b_s \frac{n}{N} \right) R_a$

……...…...…… (9)

where R_a is extraterrestrial radiation (Wm^{-2}), a_s and b_s are constant parameters that represent the amount of radiation reaching the earth, respectively, $\frac{n}{N}$ is relative sunshine duration

$R_{ns} = 0.77 R_s$ ……..…… (10)

where R_s is solar or shortwave radiation (Wm^{-2}).

$$R_{nl} = \sigma T^4 \left(0.34 - 0.14\sqrt{e_a}\right)\left(1.35\frac{R_s}{R_{so}} - 0.35\right) \quad \text{..... (11)}$$

where $\frac{R_s}{R_{so}}$ is relative shortwave radiation, σ is Stefan-Boltzmann constant ($5.67\times10^{-8} Wm^{-2}K^{-4}$).

3.3.3 Alternative ET Algorithms

In order to compare our improved ET algorithm (hereafter referred to as AL-1) to others, we adopt other two algorithms to quantify ET. One algorithm (hereafter referred to as AL-2) is based on the revised Penman-Monteith equation (Liu et al., 2013). By separating transpiration from vegetation canopy, AL-2 calculated ET in two parts from canopy and soil surface, separately:

$$ET = T_c + E_{soil} \quad \text{..... (12)}$$

where T_C is:

$$T_c = \frac{sA_c + \rho c_p \left(VPD\right)/r_a}{\lambda\left(s + \gamma\left(1 + \frac{r_s}{r_a}\right)\right)} \times sec2day \times MD \quad \text{..... (13)}$$

Where E_{soil} is:

$$E_{soil} = \frac{sA_{soil} + \rho c_p \left(VPD\right)/r_{as}}{\lambda\left(s + \gamma\left(1 + \frac{r_{tot}}{r_{as}}\right)\right)} \times sec2day \times MD \times RH^{\frac{VPD}{\beta}} \quad \text{..... (14)}$$

Where A_c (W m^{-2}) is the available energy in the vegetation canopy, A_{soil} (W m^{-2}) is the available energy in the soil, s is the slope of the saturation vapor pressure curve (Pa K^{-1}) and is a function of air temperature (kg m^{-3}); ρ is the air density, C_p (J $kg^{-1}K^{-1}$) is the specific heat capacity of air, VPD (Pa) is the vapor pressure deficit (i.e., saturated air vapor pressure minus actual air vapor pressure), r_a (s m^{-1}) is the aerodynamic resistance, r_s (s m^{-1}) is the surface resistance to transpiration from the plant canopy, r_{as} is the aerodynamic resistance at the soil surface, r_{tot} is the sum of r_{as} and surface resistance to evaporation, λ (J kg^{-1}) is the latent heat of vaporization, ρ (kg m^{-3}) is the air density, γ (Pa K^{-1}) is the psychometric constant, secs2day (s day^{-1}) is the number of seconds in a day, E_{soil_pot} is the potential evaporation from soils, f_{SM} is a proxy of soil water deficit used to constrain soil evaporation, RH is relative humidity, and β is the relative sensitivity of RH to VPD (Fisher et al., 2008). In this method, transpiration from canopy and evaporation from soil are both calculated in a similar form as P-M equation, but with different energy balance equations. ET calculated by AL-2 is then constrained by water balance in TEM.

Another algorithm (AL-3) for calculating ET is the revised algorithm from Mu et al (2011) and Son et al. (2017). In this method, evaporation from soil, wet plant and transpiration from plant are computed separately:

$$\lambda ET = \lambda E_{soil} + \lambda E_{wet\_c} + \lambda E_{trans} \quad \text{..... (15)}$$

Where E_{soil} is evaporation from soil, E_{wet_c} is transpiration from wet plant canopy surface, and E_{trans} is transpiration from plant. In this method, evaporation from snow and water bodies is also added for more accurate quantification.

3.3.4 Model parameterization, verification, and regional simulation

Site-level parameterization for ET is conducted for different PFTs at the selected sites using observational data (Table 1). Using a Markov Chain Monte Carlo (MCMC) method (Metropolis et al., 1953; Hastings, 1970), 100,000 parameter sets are generated for every PFT. For regional simulations, an optimum set of parameters for each pixel is obtained (Chen and Zhuang, 2011). To calibrate model with MODIS ET data, remote sensing data are organized to monthly and 0.5^o x 0.5^o resolution. Optimum parameters for each grid are used for ET simulations for the period 1985-2010 and future simulations. To use satellite data of ET to parameterize the model, the MCMC technique is also used in a spatially explicit manner (Chen and Zhuang, 2011). MCMC is a general method for simulation of stochastic processes with a specific probability density function. Specifically, a sequence of random variables is a Markov chain when the $(n+1)^{th}$ element only depends on the n^{th} element. The metropolis-hasting algorithm is used to generate random walk values with a proposed probability density and decide whether to accept or reject a value based on a specified acceptance ratio (Qu and Zhuang, 2017). We sample 10,000 parameter combinations for each grid in our regional calibrations.

The parameterized model is applied to estimate regional ET at a spatial resolution of $0.5^o \times 0.5^o$ from 2000 to 2010. We also conduct regional simulations with the previous version of TEM with the default parameterization in Zhuang et al. (2003). Both simulations are compared with MODIS ET product (Mu et al., 2007). ET under different representative concentration pathway (RCP) scenarios from 2016 to 2100 are also conducted.

3.4 Results

3.4.1 Comparison between simulated and observed evapotranspiration

The simulated annual ET is in a good agreement with remote sensing data (Fig. 1). Comparison between MODIS and simulated annual ET with the revised TEM indicates that they have similar spatial distributions. The difference mainly exists in low latitude areas (Fig. 2a). The Root-Mean-Square-Error (RMSE) between simulated ET with previous TEM and MODIS ET tends to be larger than that between the revised TEM and MODIS data (Fig. 2b). The RMSE for the revised TEM is 10.2 mm $month^{-1}$ and larger than 50 mm $month^{-1}$ for the previous version. The spatial distribution of ET error between two versions of the model is similar, both showing large differences in the southwest part of North America, small differences in the northern and western areas of the region.

Regional ET in North America is computed by adding each area-weighted value for all grids. Overall, annual average ET from 2000 to 2010 computed from the revised TEM agrees well with MODIS ET (RMSE less than 100 mm yr^{-1}). Largest ET is found in the southeast of North America with annual ET over 1000 mm, while most area in the east and north has ET around 200 mm per year. The spatial distribution of ET for land ecosystem types agrees well between simulations and MODIS data. Estimated ET ranges from 200 mm yr^{-1} for scrublands to 700 mm yr^{-1} for evergreen broadleaf forests.

ET in North America is generally low in winter due to low available energy, low temperature and low surface conductance. ET across North America generally increases from north to south, and the revised TEM captures the magnitude of seasonal ET variation and spatial patterns of increasing from north to south in the region. The ET in the southwestern North America has a decreasing trend, which is comparable with previous projections (Seager et al., 2007). The ET in

deciduous forest is 50% higher than ET in coniferous forest, which is consistent with findings for the western North America (Chapin et al., 2000).

The revised TEM estimated that average ET in North America is 460 mm yr^{-1} during 2000-2010, lower than the MODIS ET of 483 mm yr^{-1}. The spatial distribution of modeled ET matches well with satellite data (R^2 = 0.78) and RMSE of monthly ET is small as 8.7 mm $month^{-1}$.

ET simulation (Al-1) is compared with other algorithms including original TEM ET algorithm (Al-2) and the modified PM algorithm (Al-3) (Song et al., 2017). We also use site-level ET for calibration. In comparison with remote sensing product, Al-1 (R^2=0.82) has higher R^2 than the Al-2 (R^2=0.72) and Al-3 (R^2=0.68) for the region. Overall, the revised TEM (A1-1) better simulated ET at both site and regional levels.

3.4.2 Water availability in the historical period and during the 21st century

Water is an essential natural resource (Vörösmarty et al., 2000; Fekete et al., 2004) and also affects ecosystem carbon dynamics, especially in drought areas. Carbon uptake of ecosystems is generally thought to decrease under water-limited environment (Hunt et al., 1996). Here we estimate water availability for a region as the difference between precipitation and ET (P-ET).

During 2000-2010, monthly average P-ET is 181mm•$month^{-1}$. An increasing trend in summer (June to August) and fall (September to November) is found (Fig. 3). The seasonal average ET shows a generally decreasing trend. While monthly P-ET from 2000 to 2010 fluctuates significantly, it has a wetting trend. Seasonal P-ET for main sub-regions in North America (Alaska, Canada, the Conterminous US) are extracted (Fig. 3), from which we found annual average P-ET in Alaska and Canada are positive, while annual average P-ET in the conterminous US is negative. The inter-annual variability of P-ET shows an increase of 11.4 mm

yr^{-1} ($P < 0.1$) from 2000 to 2010. Spatially, the northwestern part of North America has a greater P-ET (213 mm $month^{-1}$) than the rest area. Grasslands and shrublands show an increasing trend, while forests show a small decreasing trend of P-ET. When compared with SMAP data (Fig. 4), simulated monthly P-ET from 2000 to 2015 is positively correlated with SMAP soil moisture (R=0.57).

During the 21st century, P-ET will decrease with increasing temperature (Fig. 5). Under an extreme climate scenario of RCP 8.5, P-ET decreases fast from 150mm $year^{-1}$ to 80mm yr^{-1} (Fig. 5b), indicating that the increase of temperature will reduce water availability in the future. Simulations for RCP scenarios 2.6 and 8.5 show different magnitudes of ET increases with an increase less than 10% in RCP 2.6 and 40% in RCP 8.5, respectively. These simulations suggest that North America tends to get drier with less water availability. By comparing the simulations under RCP 2.6 and RCP 8.5 using AL-1, we indicate that climate change with increasing CO_2 generally results in the lower water availability, which in turn affects water balance globally (Pan et al., 2015).

3.5 Discussion

3.5.1 Processes of and controls to evapotranspiration

By integrating leaf area index to ET algorithms, we manage to calibrate ET in North America in a spatially explicitly manner. To test the revised TEM, we compare it with other two algorithms. Our uncertainty analysis by varying parameters within their prior ranges is conducted with these algorithms. From 2000 to 2015, estimated regional ET in the conterminous US is 430.5±10.5 mm yr^{-1} (AL-1), 482.1±11.2 mm yr^{-1} (AL-2), and 489.7±13.4 (AL-3) mm yr^{-1}, respectively. P-ET for three algorithms are -105.3±8.7 mm yr-1, -20.3±11.9 mm yr^{-1}, -126.2±15.4 mm yr^{-1}, respectively. Al-1 estimates a decreasing trend of ET in the 21st century, while the other two algorithms show an increasing trend. When comparing the three algorithms, the main difference in ET estimates is from the ET partitioning.

ET parameters including *SLA*, *CL* and β are well calibrated. Comparing with AL-2 and AL-3, the advantage of AL-1 is that previously-calibrated LAI is well integrated into the revised model with a spatially-explicit set of parameters. ET simulations from AL-1 is more stable and closer to remote sensing product (Fig. 2). In AL-2, ET is calculated separately in terms of evaporation from soil surface and transpiration from vegetation canopy. The advantage of AL-2 is the detailed estimates of different sources of ET, but it requires more parameters to be calibrated (Fig. 6a). For AL-3, evaporation is separated for different land cover types, which also requires more parameter calibration. AL-3 is more capable of simulating ET in higher-latitude areas, where evaporation from snow is better calculated (Fig. 6b).

3.5.2 Implications of ET change to regional water resource and the climate system

To identify ET variations in different areas in North America, we simulate P-ET for sub-regions including Alaska, Canada, and four regions in the conterminous US (Northwest, Northeast, Southwest, Southeast) (Fig. 3). Annual average P-ET from 2000 to 2015 in the entire North America is negative, while Alaska has positive values, the conterminous US and Canada had negative water availability, indicating these regions have been generally dry.

Under different climate scenarios, ET variation changes water availability. Comparing with RCP8.5, ET simulation under RCP2.6 has lower ET, resulting in a persistent trend of P-ET in the 21st century, while P-ET tends to decrease under RCP8.5. Northeast US (-155.7 mm yr^{-1}) and Northwest US (-95.2 mm yr^{-1}) have lower water availability than Southeast US (26.2 mm yr^{-1}) and Southwest US (88.3 mm yr^{-1}). Comparing with southern US, northern US in the 21st century have higher precipitation and higher ET, generating combined result of lower water availability (P-ET).

Additionally, ET could influence plant productivity, affecting biomass supply and crop yield. Here we estimated plant water use efficiency (WUE) as a ratio of plant gross primary production to ET. We find that modeled WUE and observation-based WUE at site level is well correlated (R^2=0.48), with 0.68 and 0.55 for forests and grasslands, respectively. In the regions, poor correlations may result from uncertain forcing data or errors in MODIS ET product. Estimated WUE of forests and shrubland is higher than cropland and grasslands. Especially, the broadleaf forest has the highest WUE (3.5~4.5 g C g^{-1} H_2O). For most PFTs, WUE is higher in fall than in summer. Different PFTs have distinct WUE values. These results suggest that the ET is strongly related to plant production. Further, ET is a main source of water vapor to the atmosphere. From 2000-2015, the simulated ET variation (ΔET, the difference of ET between 2015 and 2000) in North America is less than 10 mm yr^{-1}. Under the RCP 2.6 and 8.5 scenarios, ET in the 21st

century increases by 110-155 mm yr^{-1}. These ET or latent heat variations will affect land surface energy balance and feedback to the climate system.

3.6 Conclusions

This study improves ET algorithms within a process-based terrestrial ecosystem model. The estimated ET with the improved model is close to MODIS monthly data. Under the RCP 2.6 and RCP 8.5 scenarios, there is an increasing trend in ET and a decreasing trend in water availability in North America. The study suggests that the region will experience a deficit of freshwater with increasing evapotranspiration in the 21st century. Our simulation biases may come from the energy budget calculation, including the computation of available energy, sunshine radiation and relative sunshine duration. Specifically, the cloudiness and aerosol conditions could affect our radiation calculation, which have not been considered. Second, the limited amount of site- and regional level observational ET data also limits our model calibration, introducing uncertainties in our regional simulations. Third, our analysis has not considered the land-use change effects.

3.7 Acknowledgement

This research was supported by a NSF project (#1028291) funded to Q.Z. We acknowledge the computing support from the Research Center for Advanced Computing at Purdue. We also acknowledge that the AmeriFlux network and MODIS provide multiple LAI, ET and other auxiliary datasets for this model-data fusion study.

Table 3.1 Key parameter values for representative ecosystem types. β represents relative sensitivity of soil moisture to vapor pressure deficit. SLA represents specific leaf area. CL represents mean potential stomata conductance

	Alpine Tundra	Wet Tundra	Boreal Forest	Temperate Coniferous Forest	Temperate Deciduous Forest	Grassland	Xeric Shrubland	Tropical Forest
β (hpa)	2.0	2.0	1.5	1.6	1.3	2.1	2.2	2.5
SLA (m^2/gC)	0.01	0.008	0.009	0.009	0.008	0.01	0.008	0.008
C_L (m/s)	0.005	0.004	0.003	0.002	0.004	0.005	0.005	0.002

(a)

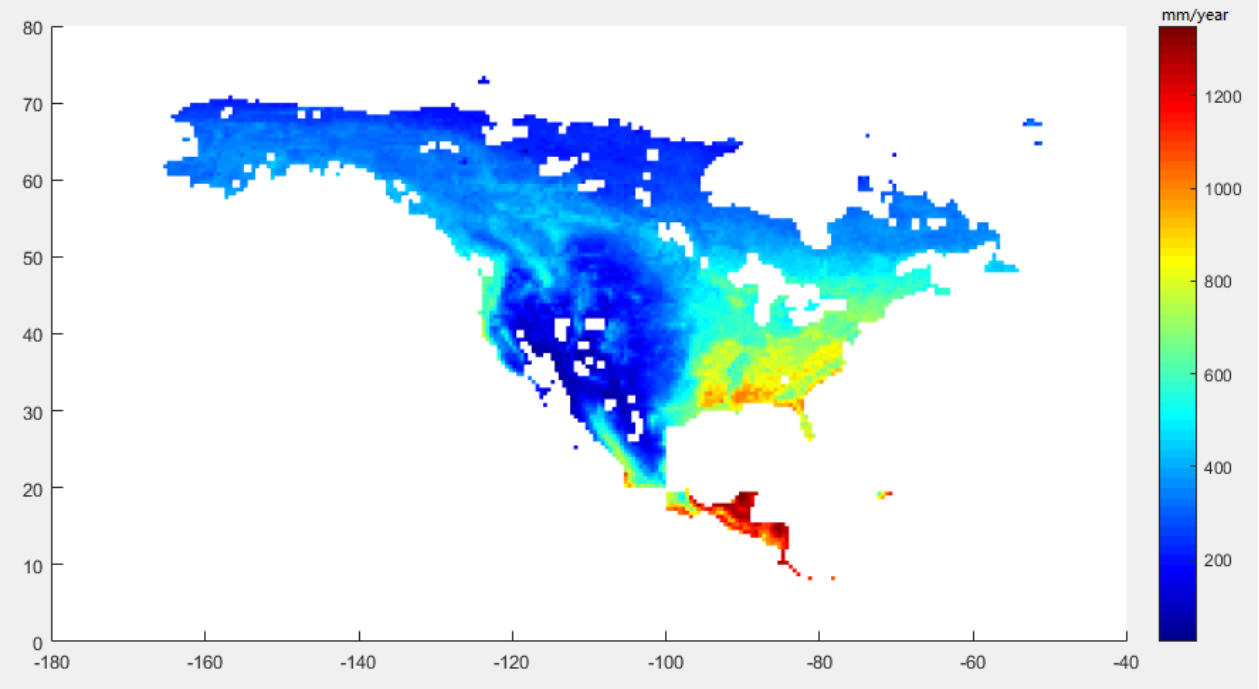

(b)

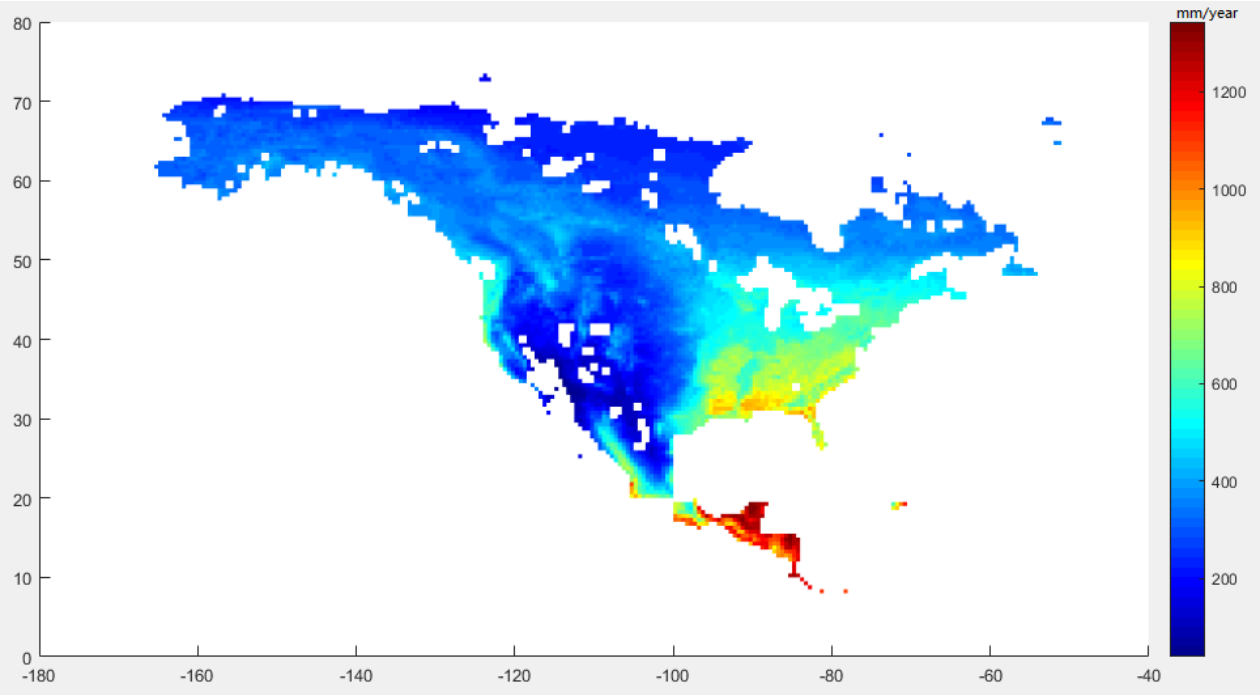

Figure 3.1 Average annual ET (mm year-1) from 2000-2010: (a) the revised TEM simulation and (b) MODIS ET product

(a)

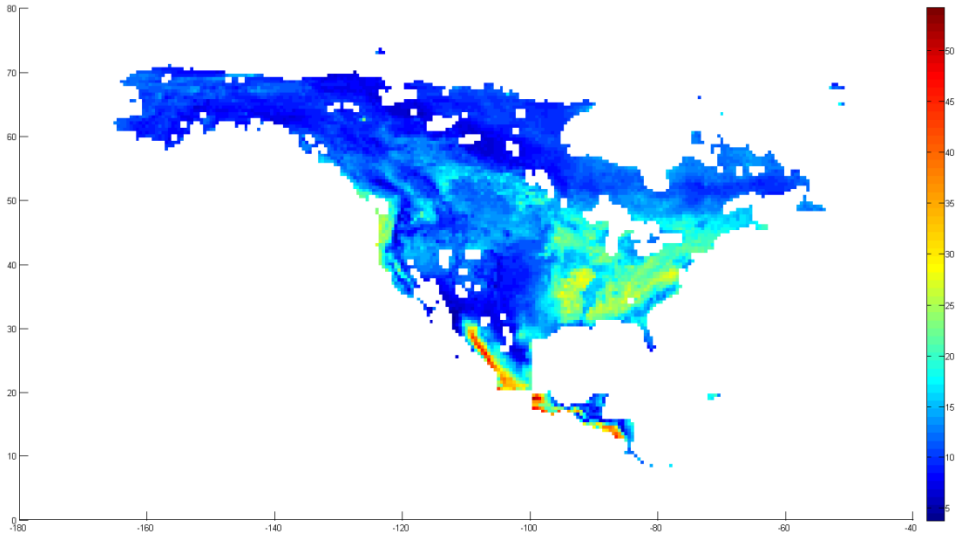

(b)

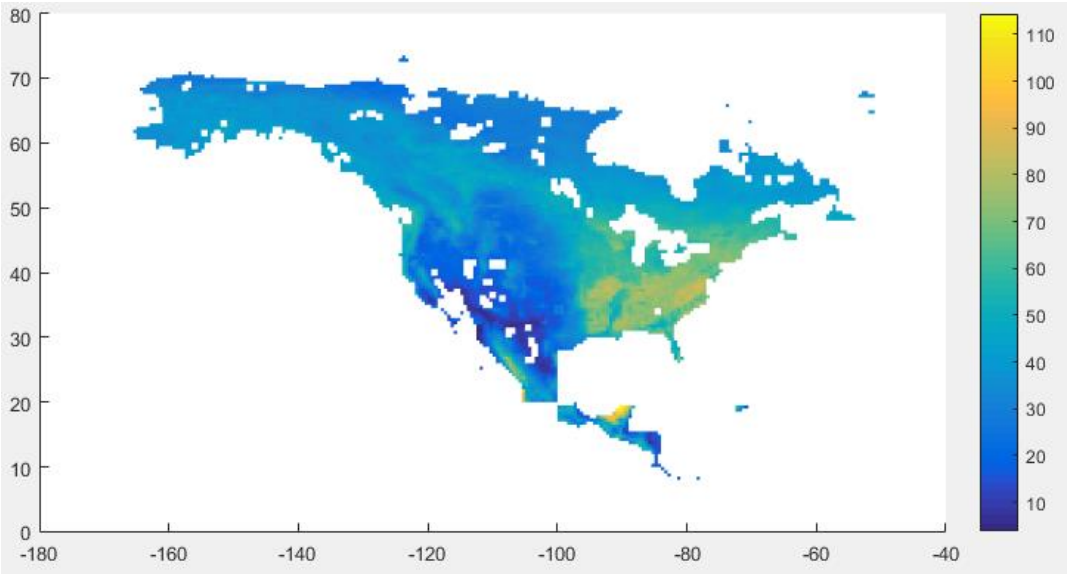

Figure 3.2 Root mean square error (RMSE) between the revised TEM simulation and MODIS ET (mm month-1) (a) and between the simulated ET using previous TEM and MODIS ET (mm month-1) (b).

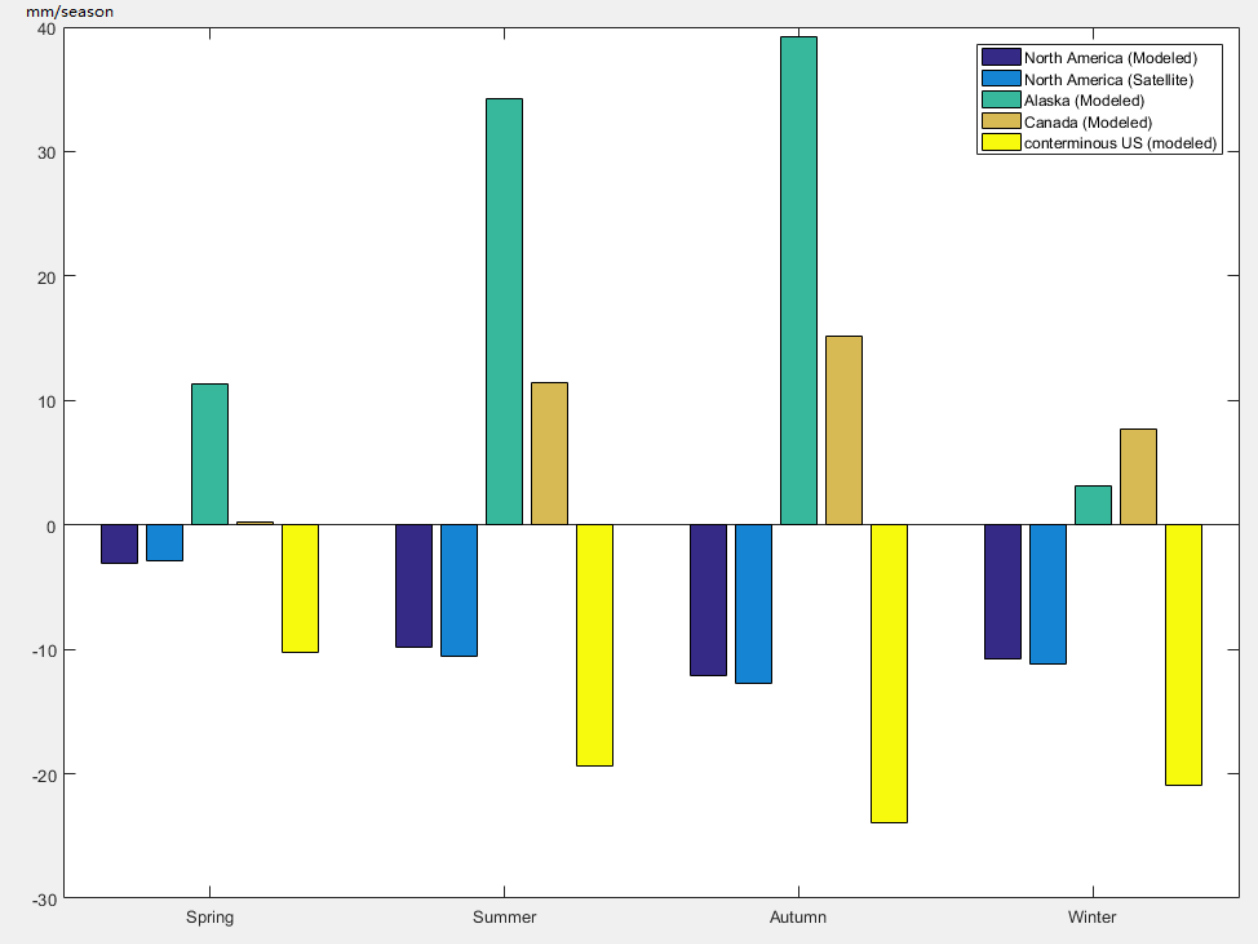

Figure 3.3 Average seasonal P-ET (mm season-1) for the period of 2000-2015 for sub-regions

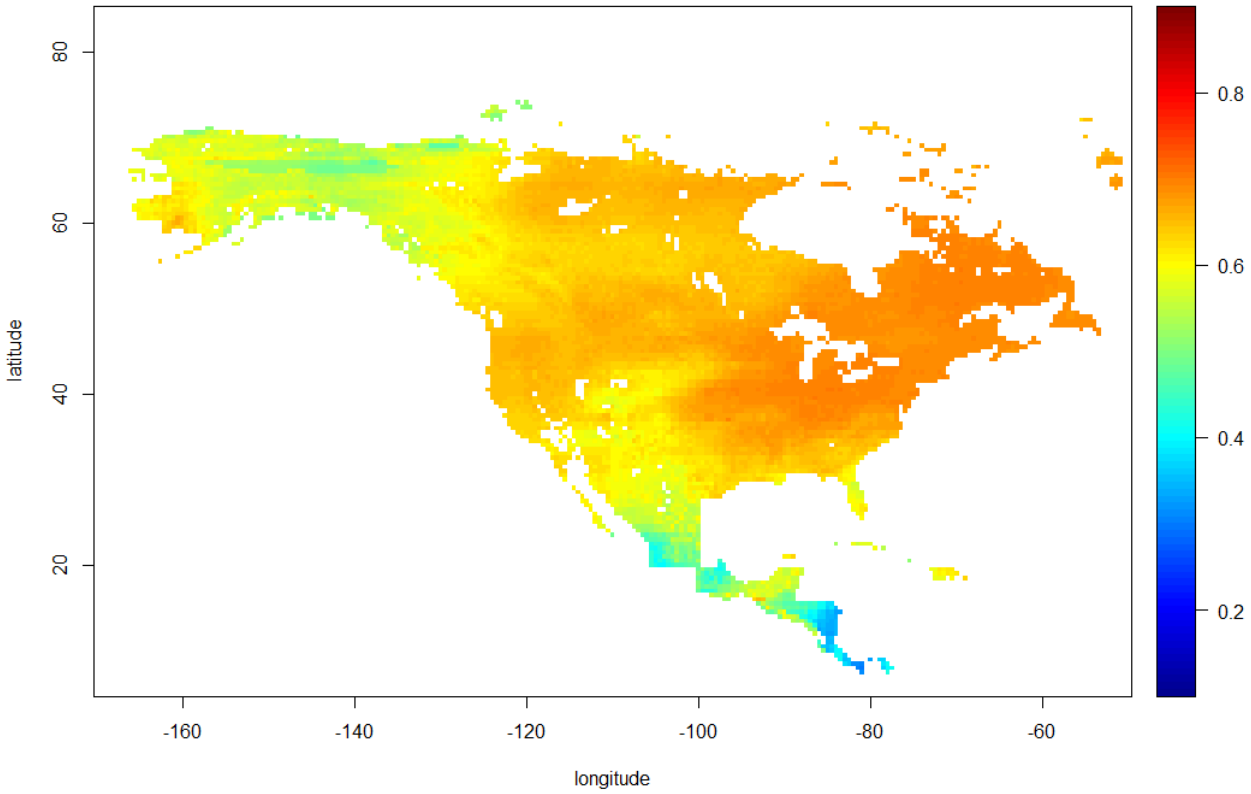

Figure 3.4 Correlations between P-ET and SMAP soil moisture

(a)

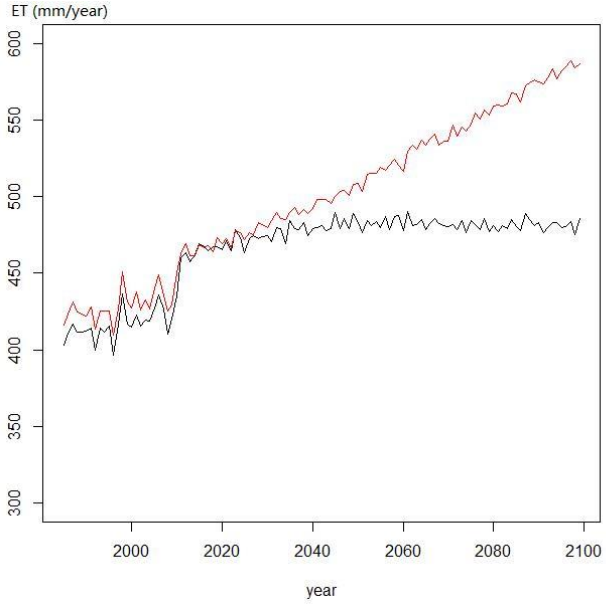

(b)

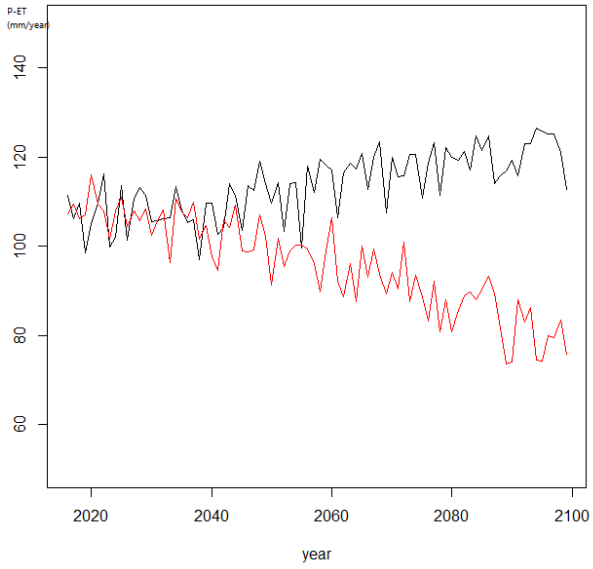

Figure 3.5 Simulated annual ET under the RCP 2.6 (black line) and the RCP 8.5 (red line) scenarios (a), and the simulated annual P-ET under RCP 2.6 (black line) and RCP 8.5 (red line) scenarios (b).

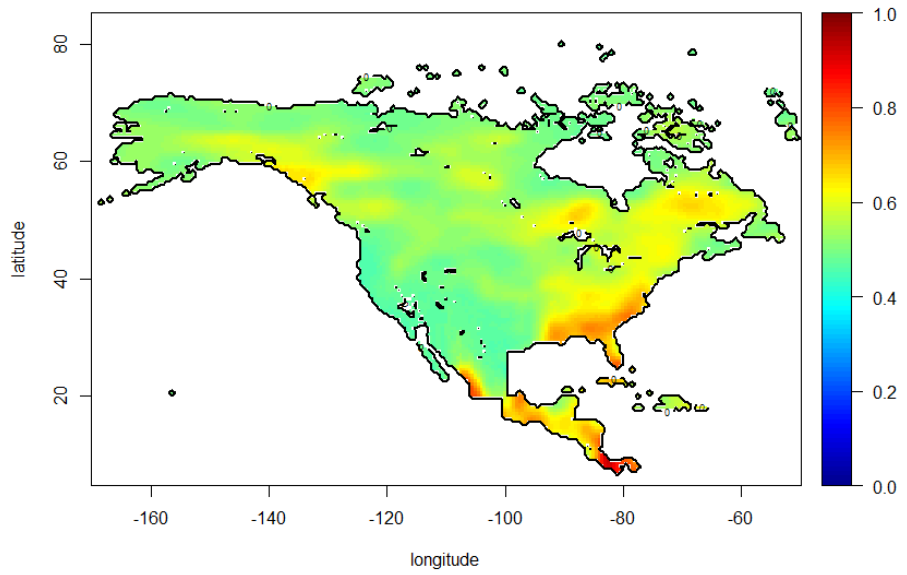

(a)

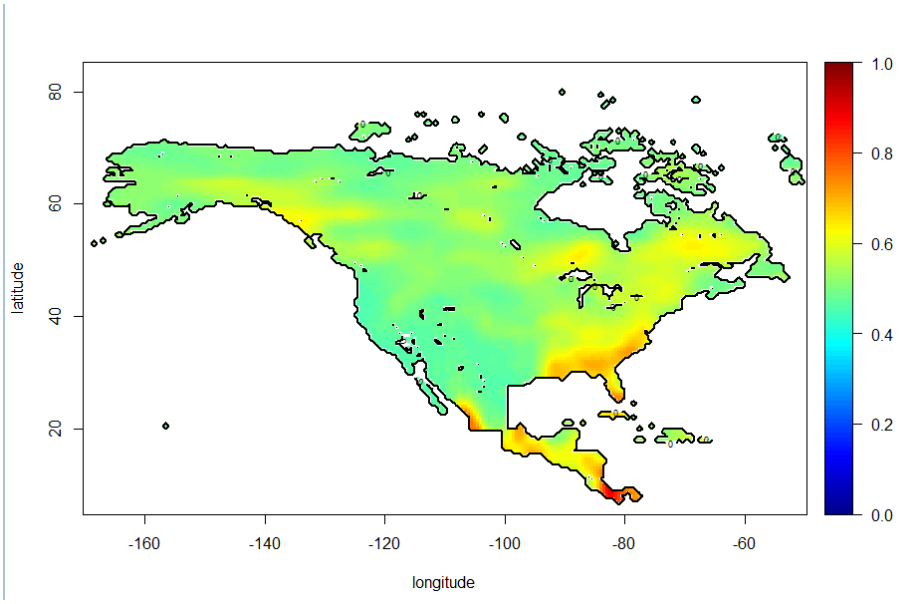

(b)

Figure 3.6 Comparisons of the estimated ET between remote sensing product and different algorithms: (a) R2 between ET from AL-2 and RS product; (b) R2 between ET from AL-3 and RS product

CHAPTER 4. AN EFFICIENT METHOD FOR ACCELERATING THE SPIN-UP PROCESS FOR PROCESS-BASED BIOGEOCHEMISTRY MODELS

4.1 Abstract

To better understand the role of terrestrial ecosystems in the global carbon cycle and their feedbacks to the global climate system, process-based biogeochemistry models need to be improved with respect to model parameterization and model structure. To achieve these improvements, the spin-up time for those differential equation-based models needs to be shortened. Here, an algorithm for a fast spin-up was developed and implemented in a biogeochemistry model, the Terrestrial Ecosystem Model (TEM). With the new spin-up algorithm, we showed that the model reached a steady state in less than 10 years of computing time, while the original method requires more than 200 years on average of model run. For the test sites with five different plant function types, the new method saves over 90% of the original spin-up time in site-level simulations. In North America simulations, average spin-up time saving for all grid cells is 85% for either daily or monthly version of TEM. The developed spin-up method shall greatly facilitate our future quantification of carbon dynamics at fine spatial and temporal scales.

4.2 Introduction

Biogeochemistry models contain state variables representing various pools of carbon and nitrogen and a set of flux variables representing the element and material transfers between different state variables. Model spin-up is a step to get biogeochemistry models to a steady state for those state and flux variables (McGuire et al., 1992; King, 1995; Johns et al., 1997;

Dickinson et al., 1998). Spin-up normally uses cyclic forcing data to force the model run, and reach a steady state, which will be used as initial conditions for model transient simulations. The steady state is reached when modeled state variables show a cyclic pattern or a constant and often requires a significant amount of computation time, which needs to be accelerated for regional and global simulations at fine spatial and temporal scales.

Spin-up is normally achieved by running model repeatedly using one or several decades of meteorological or climatic data, until a steady state is reached. The step could require model repeatedly run for more than 2000 annual cycles. Specifically, the model will check the stability of the simulated carbon and nitrogen fluxes as well as state variables with specified threshold values. For instance, the model will check if the simulated annual net ecosystem production (NEP) is less than 1 g C m^{-2} yr^{-1} (McGuire et al. ,1992). Another method to reach a steady state is to obtain the analytical solutions (King et al, 1995; Comins, 1997), which might also take a significantly long time.

For different biogeochemistry models, spin-up could take hundreds and thousands of years to reach a stability, normally longer than the model projection period (Thornton et al., 2005). Therefore, a more efficient method to reach the steady state will speed up the entire model simulation. Recently, a semi-analytical method (Xia et al., 2012) has been adapted to a carbon-nitrogen coupled model to speed up the spin-up process. The idea is to get an analytical solution very close to a steady condition, then start spin-up from the solution, which could significantly reduce spin-up time. However, this technique did not reach a cyclic pattern for state and flux variables and required an additional spin-up process to achieve the steady state.

Here we developed a new method to accelerate the spin-up process. We tested the method for representative plant function types and the North America with both daily and monthly

versions of TEM (Zhuang et al., 2003). In addition, we compared the performance of our algorithms with the semi-analytical version of Xia et al. (2012). The new algorithms shall help us conduct very high spatial and temporal resolution simulations with process-based biogeochemistry models in the future.

4.3 Method

4.3.1 Model Description

We used a process-based biogeochemistry model, the Terrestrial Ecosystem Model (TEM; Zhuang et al. 2003) as testbed to demonstrate the performance of the new algorithms of spin-up. TEM simulates the dynamics of ecosystem carbon and nitrogen fluxes and pools (McGuire et al., 1992; Zhuang et al., 2010, 2003). It contains five state variables: carbon in living vegetation (C_v), nitrogen in living vegetation (N_v), organic carbon in detritus and soils (C_s), organic nitrogen in detritus and soils (N_s), and available inorganic soil nitrogen (N_{av}). Carbon and nitrogen dynamics in TEM are governed by following equations:

$$\frac{dC_v}{dt} = GPP - R_A - L_C \quad \text{.....(1)}$$

$$\frac{dN_v}{dt} = NUPTAKE - L_N \quad \text{.....(2)}$$

$$\frac{dC_s}{dt} = L_c - R_H \quad \text{.....(3)}$$

$$\frac{dN_s}{dt} = L_N - NETNMIN \quad \text{.....(4)}$$

$$\frac{dN_{av}}{dt} = NINPUT + NETNMIN - NLOST - NUPTAKE \quad \text{.....(5)}$$

Where GPP is gross primary production, R_A is autotrophic respiration, L_C is carbon in litterfall, $NUPTAKE$ is nitrogen uptake by vegetation, L_N is nitrogen in litterfall, R_H is heterotrophic

respiration, $NETNMIN$ is net rate of mineralization of soil nitrogen, $NINPUT$ is nitrogen input from outside ecosystem, $NLOST$ is nitrogen loss from ecosystem. Key carbon fluxes are defined as:

$$GPP = C_{\max} f(PAR) f(PHENOLOGY) f(FOLIAGE) f(T) f(C_a, G_v) f(NA) f(FT) \quad (6)$$

$$NPP = GPP - R_A \quad (7)$$

$$NEP = GPP - R_A - R_H \quad (8)$$

NEP will be near zero when the ecosystem reaches a steady state. Therefore, the spin-up goal is to keep running the model driven with repeated climate forcing data until NEP is close to zero with a certain tolerance value (e.g., 0.1 g C m^{-2} yr^{-1}).

4.3.2 Spin-up acceleration method

TEM can be re-formulated as:

$$\frac{d\vec{x}}{dt} = g(\vec{x}) + \vec{h} \quad (9)$$

Where x is a vector of state variables (e.g., V_c); $\vec{h}$ is vector of carbon/nitrogen input from the atmosphere, independent on $\vec{x}$; g(x) is the process rate function of element pools (e.g., GPP).

By linearizing the model in term of pools, we could get:

$$g(\vec{x}, t) = g(\vec{x}_0, t) + J(\vec{x} - \vec{x}_0) \quad (10)$$

Where J is the Jacobian matrix of the process rate:

$$J = \frac{dg}{dx} = \begin{bmatrix} \frac{\partial g_1}{\partial x_1} & \cdot & \cdot & \cdot & \frac{\partial g_1}{\partial x_n} \\ \cdot & & & & \cdot \\ \cdot & & & & \cdot \\ \cdot & & & & \cdot \\ \frac{\partial g_n}{\partial x_1} & \cdot & \cdot & \cdot & \frac{\partial g_n}{\partial x_n} \end{bmatrix} \quad \ldots\ldots\ldots\ldots\ldots\ldots\ldots\ldots\ldots\ldots\ldots\ldots (11)$$

The numerical discretization of equation (9) is:

$$x_k - x_{k-1} = \tau \cdot J_{k-\frac{1}{2}} \cdot x_{k-1} + \tau \left(g\left(x_{0,k-1}\right) - J \cdot x_{0,k-1} + h_{k-1} \right) \ldots\ldots\ldots (12)$$

Where τ is time step (month), x_k is pool size at time k, $J_{k-\frac{1}{2}}$ is a Jacobian matrix at time step $k - \frac{1}{2}$ (half timestep).

We introduce:

$$f_{k-1} = g\left(x_{0,k-1}\right) - J \cdot x_{0,k-1} + h_{k-1} \ldots\ldots\ldots\ldots\ldots\ldots\ldots\ldots\ldots\ldots\ldots\ldots (13)$$

The equation can then be written as:

$$x_k - x_{k-1} = \tau \cdot J_{k-\frac{1}{2}} \cdot x_{k-1} + \tau \cdot f_{k-1} \ldots\ldots\ldots\ldots\ldots\ldots\ldots\ldots\ldots\ldots\ldots\ldots (14)$$

Where $J_{k-\frac{1}{2}}$ is a Jacobian matrix at time step $k - \frac{1}{2}$ (half step). After running a large number of annual cycles, model approaches a cyclo-stationary state, which can be expressed by condition $x^{T+i} = x^i$, where T is the number of time steps in one cycle. For example, when spin up is made at monthly time step using monthly climatology of temperature, precipitation and other forcing data, T equals 12, and x^1 is the size of carbon pools on January 1st, while $J^{1.5}$ is the matrix of mean process rate constants for January.

By introducing

$$A_k = \tau \cdot J_{k-\frac{1}{2}},\ y_k = \tau f_{k-\frac{1}{2}},\ B_k = I,\ C_k = I + A$$

where I is an identity matrix.

Eq. (12) can be written as:

$$-C_k \cdot x_{k-1} + B_k \cdot x_k = y_k \text{..} (15)$$

The cyclic boundary condition is: $x_1 = x_{T+1}$

Then Eq. (13) will become:

$$-C_1 \cdot x_T + B_1 \cdot x_1 = y_1 \text{..} (15a)$$

Thus equations (15, 15a) become a formulation of a linear problem with T unknown vectors x_k, which can be solved using LU decomposition or Gaussian elimination. Xia et al (2012, see Eq. 4) and Kwon and Primeau (2006) also had linear equations for a steady state, but only for annually averaged mean value. Going for annual average form reduces the size of problem, but prevents Xia et al (2012) from obtaining exact solution of the system (see their Eq. 3, 3a), because introducing cyclic boundary conditions in their Eq. (3a) was missing in their methods.

4.3.3 Numerical Implementation

Equation (15a) is explicitly expressed as:

$$\begin{pmatrix} B & 0 & 0 & 0 & 0 & 0 & -C \\ -C & B & 0 & 0 & 0 & 0 & 0 \\ 0 & -C & B & 0 & 0 & 0 & 0 \\ \cdots & \cdots & \cdots & \cdots & \cdots & \cdots & \cdots \\ 0 & 0 & 0 & -C & B & 0 & 0 \\ 0 & 0 & 0 & 0 & -C & B & 0 \\ 0 & 0 & 0 & 0 & 0 & -C & B \end{pmatrix} \times \begin{pmatrix} x^1 \\ x^2 \\ \\ \\ x^k \\ \\ x^t \end{pmatrix} = \begin{pmatrix} y^1 \\ \\ \\ \\ \\ \\ y^t \end{pmatrix}, \text{..................} (16)$$

Eq. (16) can be shown in form $Mx = Y$.

Apply the Gaussian elimination to upper block that reduces M to a lower triangular form and the elimination process is applied from right to left in the top row of M involving 2x2 blocks of matrices B, C, D and D'.

$$\begin{pmatrix} D^1 & D \\ -C_k & B_k \end{pmatrix} \begin{pmatrix} y_1 \\ y_k \end{pmatrix} \quad \text{.....(17)}$$

The result matrix is:

$$M' = \begin{pmatrix} B' & 0 & 0 & 0 & 0 & 0 & 0 \\ -C & B & 0 & 0 & 0 & 0 & 0 \\ 0 & -C & B & 0 & 0 & 0 & 0 \\ \cdots & \cdots & \cdots & \cdots & \cdots & \cdots & \cdots \\ 0 & 0 & 0 & -C & B & 0 & 0 \\ 0 & 0 & 0 & 0 & -C & B & 0 \\ 0 & 0 & 0 & 0 & 0 & -C & B \end{pmatrix} \quad \text{.....(18)}$$

The solution of eq. (15a) will be readily obtained for x.

4.3.4 Algorithm implementation to TEM

In original TEM, carbon fluxes can be defined as:

$$NPP = GPP - MR - GR \quad \text{.....(19)}$$

$$MR = V_C \cdot K_T \quad \text{.....(20)}$$

$$GR = \begin{cases} 0.25 \cdot (GPP - MR), & \text{if } GPP > MR \\ 0, & \text{otherwise} \end{cases} \quad \text{.....(21)}$$

Where net primary production (NPP) is defined as the difference of GPP and plant maintenance respiration (MR) and growth respiration (GR). MR is assumed as a function of V_C and temperature (K_T). Here we revised MR calculation:

$$MR = \begin{cases} V_C \cdot K_T, \; if \; GPP > V_C \cdot K_T \\ 0.75 \cdot V_C \cdot K_T + 0.25 \cdot GPP, otherwise \end{cases} \quad \text{.....(21)}$$

The net ecosystem production (NEP) is defined as the difference between NPP and heterotrophic respiration (R_H).

The basic workflow to implement the method is: 1) linearizing TEM first to get a sparse matrix with n-variable system; 2) performing Gaussian elimination for the linear system; 3) solving the sparse matrix to acquire the state variable values (Figure 1). To adapt this method to a daily version of TEM, we changed the cyclic condition T from 12 to 365. The other steps are the same as monthly version. We tested the new method for carbon only version and carbon-nitrogen coupled version of TEM for different PFTs (Table 1). Specifically, for the carbon only version, we only solved the differential equations that govern the carbon dynamics, while for the carbon-nitrogen coupled version, we solved the differential equations that govern both carbon and nitrogen dynamics in the system. For the both versions, the spin-up process strives to reach a steady state for carbon pools and fluxes.

4.4 Results and Discussion

At Harvard Forest site, the traditional spin-up method took 564 years to get the steady state for both the carbon-only and coupled carbon–nitrogen simulations with annual NEP less than 0.1 g C m^{-2} yr^{-1} (Figure 2). The improved method took 72 years for the carbon only and 122 for the coupled carbon–nitrogen simulations, respectively. For carbon and nitrogen pools, it took another 45 years (equivalent cyclic time) to reach a steady state with NEP less than 0.1 g C m^{-2} yr^{-1}. In comparison with the traditional spin-up method (Zhuang et al., 2003), the new method saved 65% of computational time to get the steady state in the carbon-only simulations (Table 2). The differences in steady-state carbon pools between using the new method and traditional spin-

up methods were small (less than 0.85%). Similarly, for the coupled carbon–nitrogen simulations, the new method saves a similar amount of time to reach the steady state. For the seven test sites, it takes on average 0.6 seconds using new method to reach a steady state. Compared to the original spin-up method, the new method is not only faster, but also computationally stable.

The time of spin-up to reach a steady state of NEP varied for different PFT grids using the original method (Figure 2). In general, to allow 98% grid cells reach their steady states of NEP, it will take 250 annual model runs. While the new method will only need on average 0.6 seconds (equivalent to 60-year annual model runs with the original method) (Figure 3). For regional tests in North America, we found that the average saving time with the new method with monthly TEM is 25%, 32%, and 22%, for Alaska, Canada, and the conterminous US, respectively.

To compare the performance of the new method with other existing methods, we adapted the semi-analytical method (Xia et al., 2012) to TEM model. To do that, we first revised the TEM model structure to:

$$\frac{dP(t)}{dt} = \varepsilon ACP(t) \quad \ldots\ldots\ldots\ldots\ldots\ldots\ldots\ldots\ldots\ldots (22)$$

Where P(t) is a vector of pools in TEM (e.g., V_C and S_C). ε is a scalar. A is a pool transfer matrix (in which A_{ij} represents the fraction of carbon transfer from pool j to i). C is a diagonal matrix with pool components (where diagonal components quantify the fraction of carbon left from the state variables after each time step). With this method, we obtained an analytical solution for the intermediate state. We then kept running TEM with the traditional spin-up process. Specifically, we started TEM simulation to estimate the state variable values. Based on these values, the spin-up runs were conducted to reach the final steady state. We found that the semi-analytical solution

is better than the original spin-up method, but slower than the new method proposed in this study (Table 2).

4.5 Summary

We developed a new method to speed up the spin-up process in process-based biogeochemistry models. We found that the new method shortened 90% of the spin-up time using the traditional method. For regional simulations in North America, average spin-up time saving is 85% for either daily or monthly version of TEM. This method will significantly help our future carbon dynamics quantification with biogeochemistry models at fine spatial and temporal scales.

Table 4.1 Test sites for new spin-up algorithms

Site Name	Location	PFT	Reference
1. Fort Peck	48.3N, 105.1W	Grassland	Gilmanov et al. [2005]
2. Bartlett Exp Forest	44.1N, 71.3W	Deciduous broadleaf	Ollinger et al. [2005]
3. UCI_1850	55.9N, 98.5W	Evergrenn needle-leaf	Goulden et al. [2006]
4. Vaira Ranch	38.4N, 121.0W	Grassland	Baldocchi et al. [2004]
5. Missouri Ozark	38.7N, 92.2	Deciduous broadleaf	Gu et al. [2007, 2012]
6. Niwot Ridge	40.0N, 105.5W	Evergrenn needle-leaf	Turnipseed et al. [2003, 2004]
7. Harvard Forest	43.5N, 72.2W	Deciduous broadleaf	Van Gorsel et al. [2009]

Table 4.2 Spin-up time comparison for different methods, seconds represent real computation time, years refer to the spin-up annual cycles

Site No.	Original Spin-up Year	Spin-up computation time (Seconds)	New method computation time (Seconds)	Semi-analytical method (equivalent annual cycles)
1	231	1.3	0.5	0.7s (+76)
2	305	1.7	0.3	0.8s (+101)
3	245	1.5	0.4	0.9s (+52)
4	443	2.2	0.4	0.5s (+118)
5	304	1.8	0.4	0.8s (+86)
6	204	1.1	0.3	0.7s (+43)
7	564	2.5	0.6	0.9(+45)

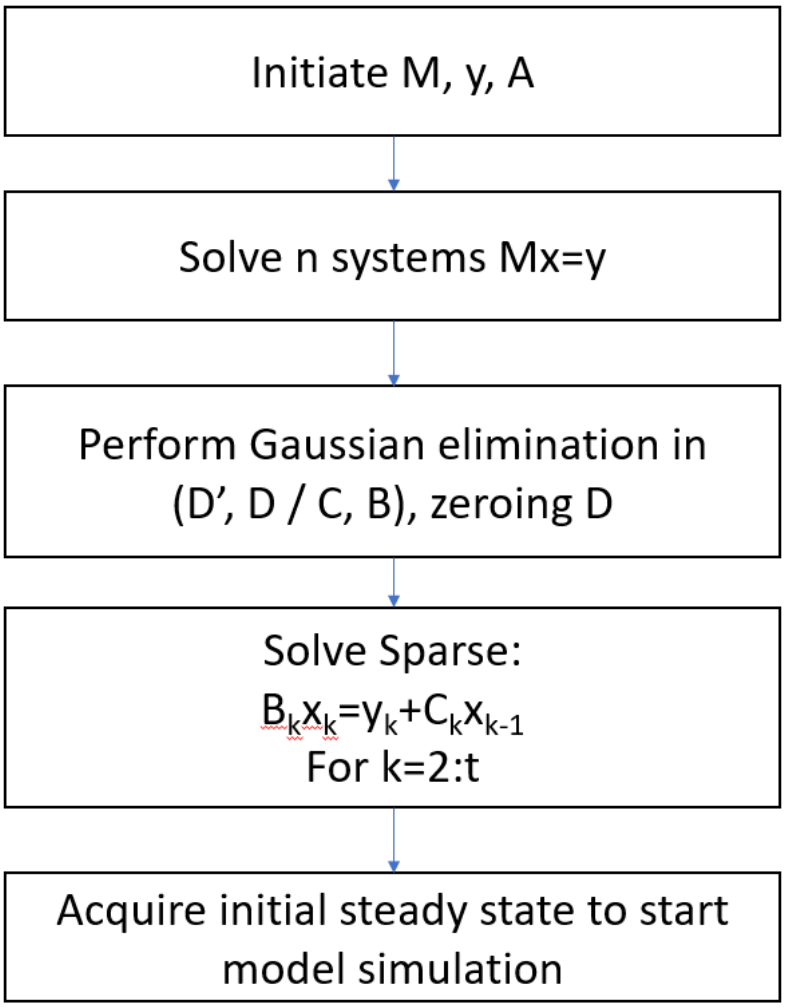

Figure 4.1 Algorithms and procedures of the new spin-up method

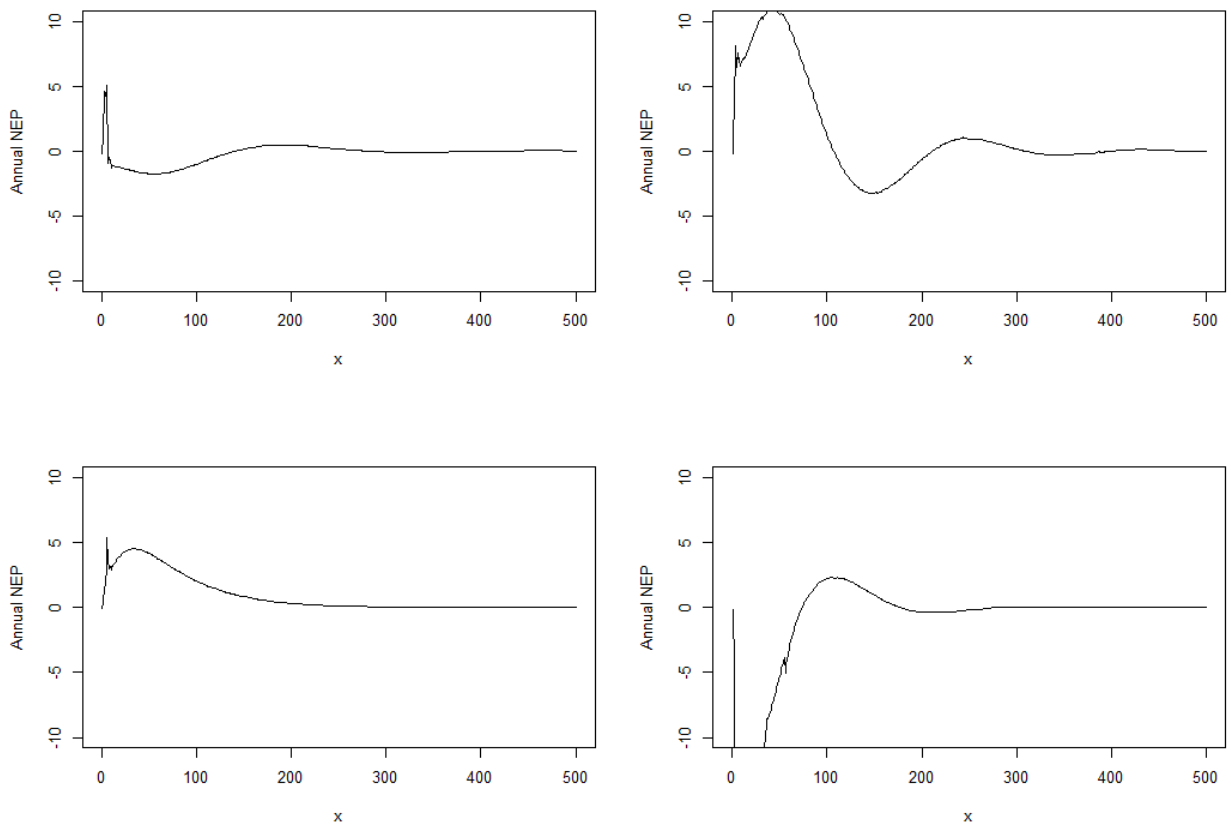

Figure 4.2 The time for NEP (g C $yr^{-1}m^{-2}$) reached a steady state with the original spin-up method at Harvard forest site. x represents model simulation years.

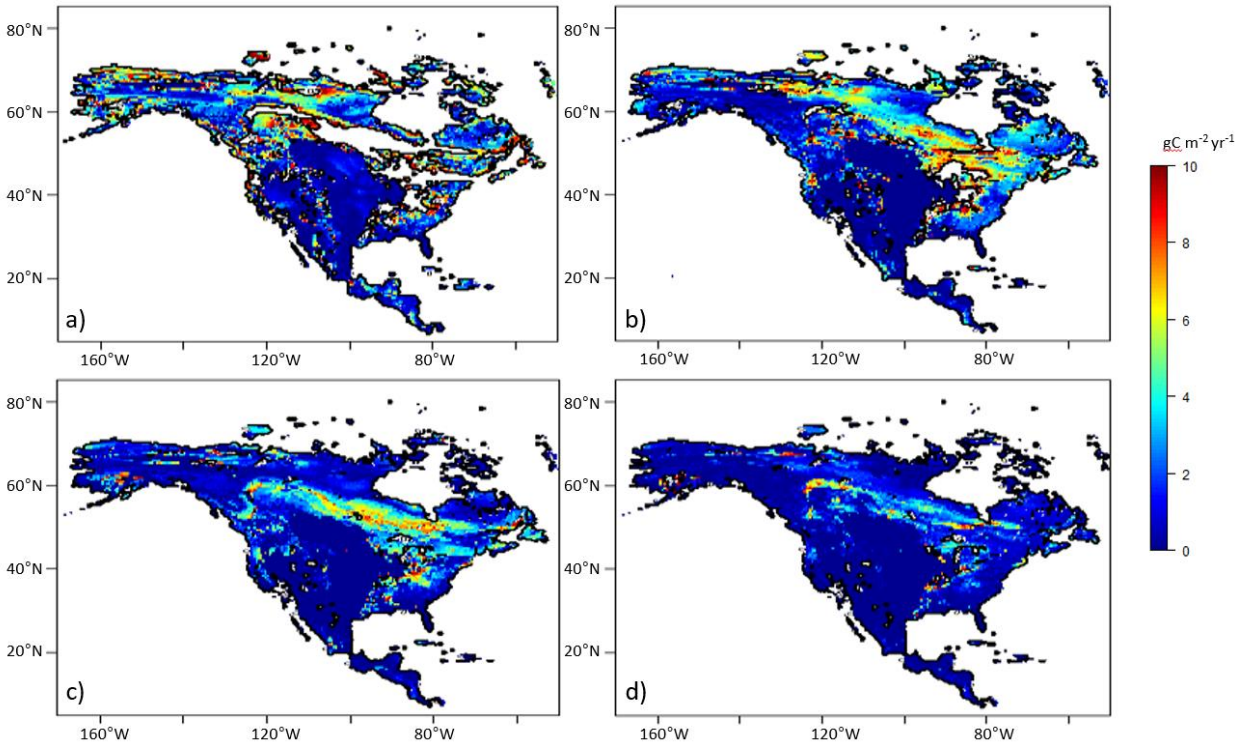

Figure 4.3 The spin-up time to reach the steady state of NEP (g C m^{-2} yr^{-1}) with the original spin-method: In 50, 100, 150, and 200 years, 63%, 89%, 93%, and 98% grids will reach their steady states, respectively.

CHAPTER 5. EVALUATING CARBON DYNAMICS OF THE CONTERMINOUS US USING DIFFERENT SPATIAL RESOLUTION MODELS AND SATELLITE DATA

5.1 Abstract

To better understand the role of terrestrial ecosystems in the global carbon cycle and their feedbacks to the global climate system, process-based ecosystem models that are used for quantifying net carbon exchanges between the terrestrial biosphere and the atmosphere need to be improved. In this chapter, we improved a process-based biogeochemistry model by increasing spatial resolution (from 0.5 degree to 0.05 degree), adopting a faster spin-up algorithm, and using high-performance computing facilities. I conducted simulations under both original resolution and high resolution for the conterminous US. Simulations show that the high-resolution simulation predicts slightly higher annual gross primary production (GPP) (~2%) from 2000 to 2015 in the Conterminous US than the low-resolution simulation. The high-resolution simulations estimate that regional GPP is between 7.12 and 7.69 Pg C yr^{-1} and NEP is between 0.09 and 0.75 Pg C yr^{-1}, while MODIS product show the average GPP is 6.2 Pg C yr^{-1} and NPP is 3.3 Pg C yr^{-1}.

5.2 Introduction

Various resolutions of biogeochemistry models have been developed to quantify carbon fluxes (Bonan et al., 2002; DeFries et al., 2002). However, there are less studies to focus on analyzing how different spatial resolutions of simulations will differ in the regional and global carbon budget. Here I use a process-based ecosystem model, the Terrestrial Ecosystem Model (TEM; Zhuang et al. 2003, 2010), to analyze the simulation differences by applying the model at different spatial resolutions. TEM is a process-based model that quantifies the dynamics of carbon, nitrogen, water, and energy at a monthly time step, using spatially-explicit data of vegetation, climate, soil and elevation (Raich et al. 1991, McGuire et al. 1992, Melillo et al. 1993, Felzer et al. 2004, Zhuang et al. 2001, 2002, 2003, 2010). TEM consists of a set of ordinary differential equations that govern the exchanges of carbon and nitrogen between soils, vegetation, and the atmosphere. Here I also take advantage of available site-level and satellite-based observation data to fully calibrate TEM parameters for gross primary production quantification under different spatial resolutions. The model is then used to conduct GPP simulations for natural ecosystems in the conterminous US. The remote sensing products for the entire region and various plant function types (PFTs) are used to evaluate the model.

This study also uses the developed fast spin-up method (Chapter 3) to parameterize the model for each pixel, and to conduct the regional simulation at high-resolution. My research hypotheses are: 1) fast spin-up method can accelerate our model parameterization for a region; 2) high-resolution simulations better estimate GPP/NPP in comparison with low-resolution simulations and satellite data. In addition, the regional net ecosystem production is also quantified at different spatial resolutions for the period from 2000 to 2015.

5.3 Method

5.3.1 Model and data

I used a process-based biogeochemistry model, the Terrestrial Ecosystem Model (TEM; Zhuang et al. 2003) as testbed to demonstrate the performance of the new algorithms of spin-up. TEM simulates the dynamics of ecosystem carbon and nitrogen fluxes and pools (McGuire et al., 1992; Zhuang et al., 2010, 2003). It contains five state variables: carbon in living vegetation (C_v), nitrogen in living vegetation (N_v), organic carbon in detritus and soils (C_s), organic nitrogen in detritus and soils (N_s), and available inorganic soil nitrogen (N_{av}). Carbon and nitrogen dynamics in TEM are governed differential equations describing how element fluxes related with each pool.

To quantify carbon dynamics in the conterminous US, I organized global monthly climate data for the period 1985-2010 at a spatial resolution of 0.05°×0.05° including soil, topography and climate data. In addition, data of soil texture, elevation, and plant function types (PFT) at the same spatial resolution are also used (Zhuang et al., 2003). Land cover information (PFTs) is not specifically classified since we generate spatially-explicit parameters sets for every individual grid. Monthly mean climate data are from original NCEP datasets with resolution of 0.5°×0.5°, and then interpolated to 0.05°×0.05° to match MODIS product of GPP and NPP (Zhao et al., 2005).

5.3.2 Spatially explicit parameters for the conterminous US

I parameterize the high-resolution TEM using the MCMC method (Qu and Zhuang, 2018) in a spatially-explicit manner. For each grid, 15 parameters (Table 1) are improved from 100,000 sampling sets. The initial parameters are from previous studies (McGuire et al., 1992;

Zhuang et al., 2003). After parameterizing the high-resolution TEM, I conduct simulation for the conterminous US from 2000 to 2015 at 0.05 degree spatial resolution and monthly time step. The spin-up process is improved using the developed technique (Qu et al., 2018) where initial state of pools is computed directly. I then run the original TEM at 0.5 degree spatial resolution for comparison.

5.3.3 Spatial and temporal resolution analysis

Here I describe how model simulations are conducted at 0.05-by-0.05-degree resolution, which is 100 times of the original half-by-half degree resolution. I assume that the finer resolution should have better accuracy in mapping distribution of carbon fluxes, and better visualizing carbon sink and source activities. The higher resolution model not only describes land cover better, but also benefits the analysis for PFTs and sub-regions. Continuous mapping of carbon fluxes in two different resolutions are compared in a wall-to-wall manner, to see how different spatial resolutions affect overall results over time.

5.4 Results and Discussion

5.4.1 Spatial comparison between TEM simulations and Satellite Data

TEM simulations at the high resolution show that the GPP is between 7.12 and 7.69 Pg C yr^{-1} and NEP is between 0.09 and 0.75 Pg C yr^{-1}. MODIS GPP product estimates that the average annual GPP is 5.82 Pg C yr^{-1}. While our simulated GPP is higher than MODIS GPP, but they are significantly correlated (r^2=0.71, P<0.001).

As an essential carbon flux, NPP is calculated as the difference between GPP and plat respiration (R_A). NPP can be used to address fundamental ecosystem goods and service questions, such as bioenergy supply, food supply, deforestation, and desertification, by

evaluating changes of NPP. Indeed, terrestrial NPP is regularly identified as a key variable for various ecological monitoring activities (Niemeijer 2002). Our high-resolution model predicted annual NPP is from 3.1 to 3.6 Pg C yr^{-1} during our study period. The spatial distribution information of our estimated NPP shall help the analysis of bioenergy, food, and biomass supply in the US.

5.4.2 Temporal comparison between model simulations and satellite data of GPP/NPP

For satellite data to have value for land management, the resolution must be sufficient to resolve major ownership and ecotonal boundaries. High resolution version of GPP and NPP data stream needs to be developed for the continental United States to provide a high-resolution GPP and NPP for land management.

A specific example is, for agricultural economics, traders care about how crops are growing in competing areas worldwide. Traditionally, MODIS GPP has been effectively used for the estimation of wheat yield (Reeves et al., 2004). But for no-satellite data era, our estimated spatially and temporally varied NPP shall facilitate these activities.

In addition, I compare monthly NPP values from high-resolution simulations, low-resolution simulations and satellite product (Figure 4.3). High-resolution NPP is slightly higher (2.2%) than low-resolution NPP in the conterminous US while MODIS NPP product is lower than model simulations. Annual MODIS NPP is 58% of high-resolution NPP simulated with TEM.

5.5 Summary

I conduct GPP and NPP simulations for natural ecosystems in the conterminous US at different spatial resolutions. The remote sensing products for the entire region and various plant

function types (PFTs) are used to evaluate the model. I found that the high-resolution simulation predicts slightly higher average annual GPP from 2000 to 2015 in the conterminous US than the low-resolution simulations. High-resolution simulations show that regional GPP is between 7.12 and 7.69 Pg C yr^{-1} while low-resolution simulations show that GPP ranging from 7.01 to 7.73 Pg C yr^{-1} . Overall, my analysis for the conterminous US shows that the spatial resolutions make a small difference in regional GPP estimates (~2%).

Table 5.1 Parameters Calibrated in TEM

Parameter	Definition
k_i	Half saturation constant for PAR used by plants
k_c	Half saturation constant for CO_2-C uptake by plants
RAQ10A0	Leading coefficient of the Q10 model for plant respiration
RAQ10A1	1st order coefficient of the Q10 model for plant respiration
RAQ10A2	2nd order coefficient of the Q10 model for plant respiration
RAQ10A3	3rd order coefficient of the Q10 model for plant respiration
RHQ10	Change in heterotrophic respiration rate due to 10 °C temperature increase
MOISTOPT	Optimum soil moisture content for heterotrophic respiration
C_{max}	Maximum rate of photosynthesis C
K_r	Logarithm of plant respiration rate at 0 °C
K_d	Heterotrophic respiration rate at 0°C
KFALL	Proportion of vegetation carbon loss as litterfall monthly
N_{max}	Maximum rate of N uptake by vegetation
N_{up}	Ratio between N immobilized and C respired by heterotrophs
NFALL	Proportion of vegetation nitrogen loss as litter-fall monthly

(a)

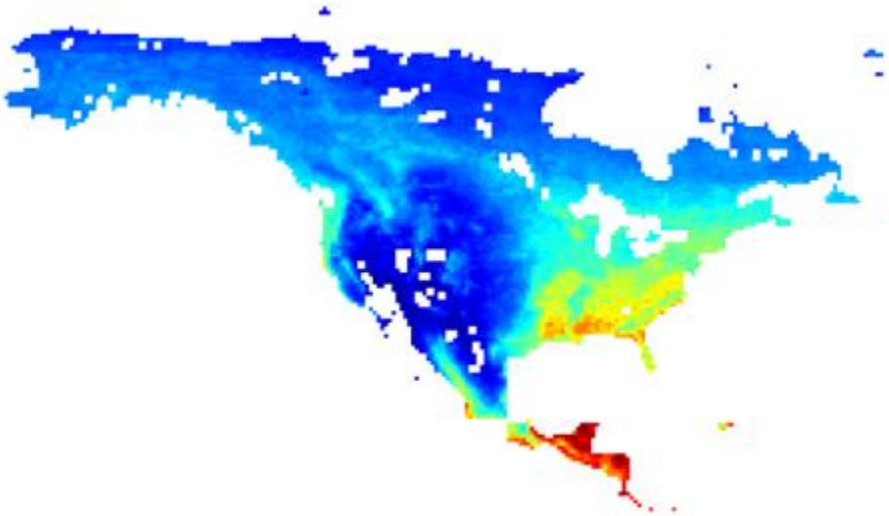

(b)

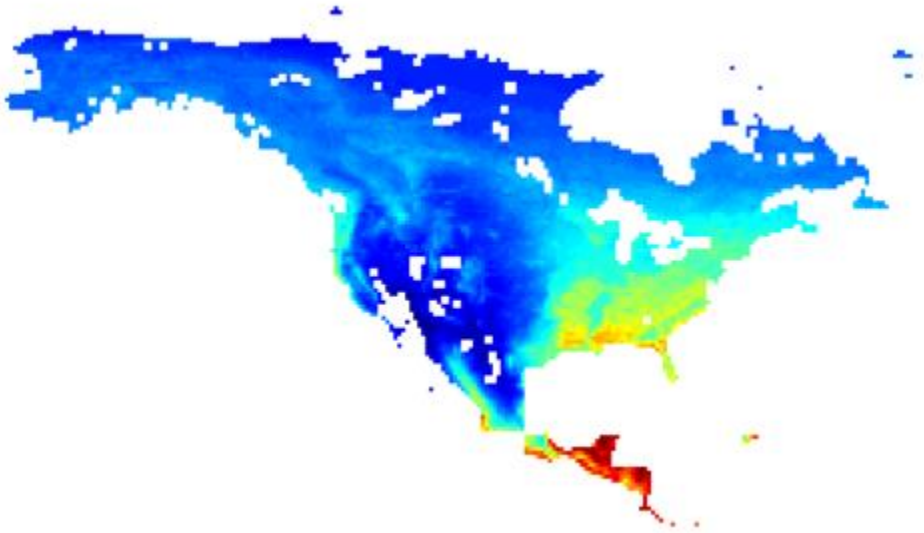

Figure 5.1 Comparison between mean annual GPP for 2000-2015 under (a) low resolution and (b) high resolution

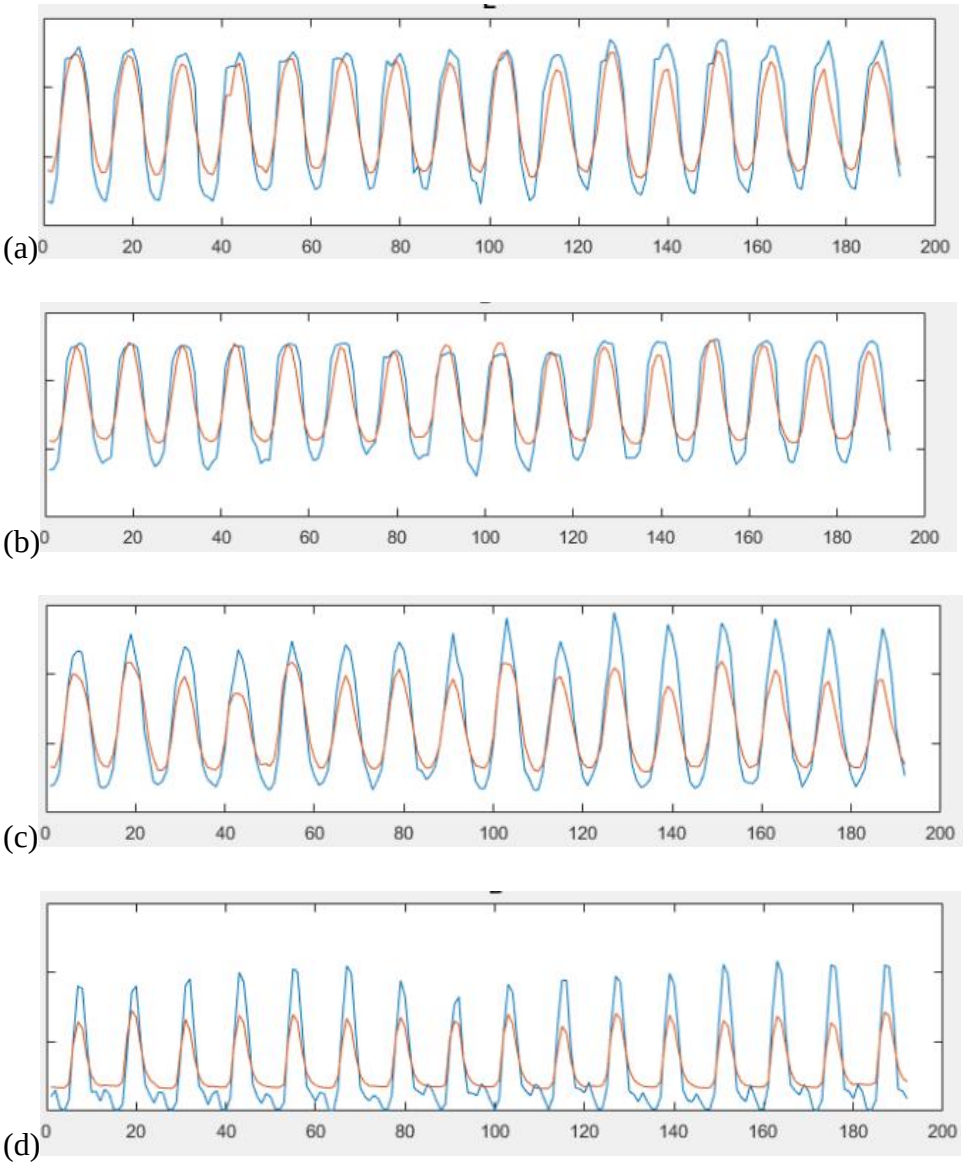

Figure 5.2 Comparison of simulated monthly GPP in the conterminous US under two different resolutions, categorized by plant functional types

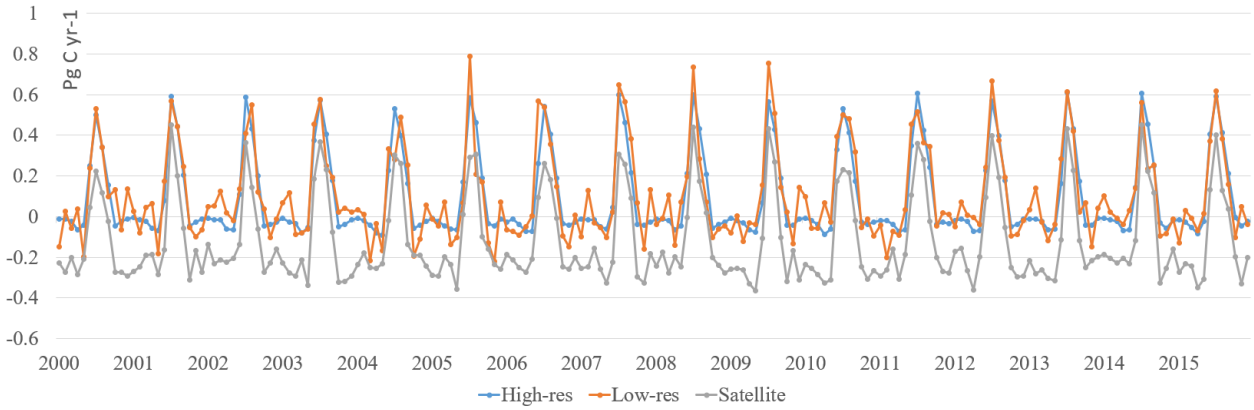

Figure 5.3 Comparison of monthly NPP simulated at high-resolution and low-resolution as well as satellite NPP product

CHAPTER 6. SUMMARIES AND FUTURE WORK

This dissertation improves the quantification of carbon dynamics and hydrologic model in a process-based ecosystem modeling framework. In situ and remote sensing data are used to improve model structure as well as parameterization. A new algorithm to increase the spin-up of the process-based models is developed and applied to finer spatial and temporal resolution simulations.

In chapter 2, I use observational LAI data from AmeriFlux network to optimize parameters at the site level. Remote sensing data of AVHRR LAI product is used to optimize parameters at regional scales. Comparison between model simulations and satellite-based LAI for the region shows that the model is able to estimate the seasonality and interannual variability of LAI in the region. The LAI in recent three decades has increased by 3% on average in the region. The simulated monthly average LAI increase during study period was 1.24, 1.46 and 2.21 m^2m^{-2}, in Alaska, Canada, and the conterminous US, respectively, which is consistent with satellite observations. In comparison with satellite data, the model captured the phenology change for key plant functional types from 1985 to 2010. The model also performed well to capture the regional phenology change in Alaska, Canada, and the conterminous US. This study provides a way to estimate the changes of leaf area index and phenology, which will improve future carbon and water cycling quantification for the region.

In chapter 3, I improve ET algorithms within a process-based terrestrial ecosystem model. The estimated ET with the improved model is close to MODIS monthly data. Under the RCP 2.6 and RCP 8.5 scenarios, there is an increasing trend in ET and a decreasing trend in water availability in North America. The study suggests that the region will experience a deficit of freshwater with increasing evapotranspiration in the 21st century. My simulation biases may

come from the energy budget calculation, including the computation of available energy, sunshine radiation and relative sunshine duration.

In chapter 4, I developed a new method to speed up the spin-up process in process-based biogeochemistry models. I found that the new method shortened 90% of the spin-up time using the traditional method. For regional simulations in North America, average spin-up time saving is 85% for either daily or monthly version of TEM.

In chapter 5, I improved TEM with a fast spin-up technique at higher spatial resolution. The remote sensing products for the entire region and various plant function types (PFTs) are used to evaluate the model. The different distribution of parameters is mapped and compared internally.

For the future work, first, I will include integrating the improved LAI modeling into the quantification of carbon cycling. Specifically, with our spatial-explicitly calibrated LAI, I shall be able to improve gross primary production simulations, thus net primary production (NPP) and net ecosystem production defined as the difference of NPP and heterotrophic respiration. Second, with better representation of phenology in TEM, I will further calibrate all other parameters related to carbon dynamics, using EnKF or adjoint method (Zhu and Zhuang, 2013) to improve carbon modeling, with the help from my fast spin-up method. Third, I will check how LAI can be better modeled considering more environmental factors. Currently I modeled LAI as a function of vegetation carbon only. Finally, the high-resolution version of TEM has more potentials to be applied for the global analysis of carbon dynamics, especially with its fast spin-method and better algorithms of LAI.

REFERENCES

Allen, R. G. (2000). Using the FAO-56 dual crop coefficient method over an irrigated region as part of an evapotranspiration intercomparison study. Journal of Hydrology, 229(1), 27-41.

Allen, R. G., L. S. Pereira, D. Raes., and M. Smith. 1998. Crop Evapotranspiration-Guidelines for computing crop water requirements-FAO Irrigation and drainage paper 56. FAO, Rome 300(9).

Allen, R. G., Tasumi, M., Morse, A., & Trezza, R. 2005. A Landsat-based energy balance and evapotranspiration model in Western US water rights regulation and planning. Irrigation and Drainage Systems, 19(3-4), 251-268.

Anav, A., G. Murray-Tortarolo, P. Friedlingstein, S. Sitch, S. Piao, and Z. Zhu. 2013. Evaluation of land surface models in reproducing satellite Derived leaf area index over the high-latitude northern hemisphere. Part II: Earth system models. Remote Sensing 5(8): 3637-3661.

Arora, V. K., and G. J. Boer. 2005. A parameterization of leaf phenology for the terrestrial ecosystem component of climate models. Global Change Biology 11(1): 39-59.

Asner, G. P., J. M. Scurlock, and J.A. Hicke. 2003. Global synthesis of leaf area index observations: implications for ecological and remote sensing studies. Global Ecology and Biogeography 12(3): 191-205.

Asrar, G., Fuchs, M., Kanemasu, E. T., & Hatfield, J. L. 1984. Estimating absorbed photosynthetic radiation and leaf area index from spectral reflectance in wheat. Agronomy journal, 76(2), 300-306.

Asrar, G., Myneni, R. B., Li, Y., & Kanemasu, E. T. 1989. Measuring and modeling spectral characteristics of a tallgrass prairie. Remote Sensing of Environment, 27(2), 143-155.

Balzarolo, M., S. Vicca, A. L. Nguy-Robertson, D. Bonal, J. A. Elbers, Y. H. Fu, ... and A. Suyker. 2016. Matching the phenology of net ecosystem exchange and vegetation indices estimated with MODIS and FLUXNET in-situ observations. Remote Sensing of Environment 174: 290-300.

Baret, F., & Guyot, G. 1991. Potentials and limits of vegetation indices for LAI and APAR assessment. Remote sensing of environment, 35(2), 161-173.

Baret, F., Hagolle, O., Geiger, B., Bicheron, P., Miras, B., Huc, M., Berthelot, B., Niño,F.,Weiss, M., Samain, O., Roujean, J. L. & Leroy, M. 2007. LAI, fAPAR and fCover CYCLOPES global products derived from VEGETATION: Part 1: Principles of the algorithm. Remote sensing of environment, 110(3), 275-286.

Baret, F., O. Hagolle, B. Geiger, P. Bicheron, B. Miras, M. Huc, B. Berthelot, F. Niño, M. Weiss, O. Samain, J. L. Roujean, and M. Leroy. 2007. LAI, fAPAR and fCover CYCLOPES global products derived from VEGETATION: Part 1: Principles of the algorithm. Remote sensing of environment 110(3): 275-286.

Barichivich, J., K. R. Briffa, R. B. Myneni, T. J. Osborn, T. M. Melvin, P. Ciais, ... and C. Tucker. 2013. Large-scale variations in the vegetation growing season and annual cycle of atmospheric CO2 at high northern latitudes from 1950 to 2011. Global change biology 19(10): 3167-3183.

Beaubien, E. G., and H. J. Freeland. 2000. Spring phenology trends in Alberta, Canada: links to ocean temperature. International Journal of Biometeorology 44(2): 53-59.

Beck, P. S., Atzberger, C., Høgda, K. A., Johansen, B., & Skidmore, A. K. 2006. Improved monitoring of vegetation dynamics at very high latitudes: A new method using MODIS NDVI. Remote sensing of Environment, 100(3), 321-334.

Betts, A. K., Ball, J. H., Beljaars, A., Miller, M. J., & Viterbo, P. A. 1996. The land surface-atmosphere interaction: A review based on observational and global modeling perspectives. Journal of Geophysical Research: Atmospheres, 101(D3), 7209-7225.

Bey, I., Jacob, D. J., Yantosca, R. M., Logan, J. A., Field, B. D., Fiore, A. M., ... & Schultz, M. G. 2001. Global modeling of tropospheric chemistry with assimilated meteorology: Model description and evaluation. Journal of Geophysical Research: Atmospheres, 106(D19), 23073-23095.

Biederman, J. A., Scott, R. L., Goulden, M. L., Vargas, R., Litvak, M. E., Kolb, T. E., ... & Garatuza-Payan, J. 2016. Terrestrial carbon balance in a drier world: the effects of water availability in southwestern North America. Global change biology, 22(5), 1867-1879.

Burrows, S. N., S. T. Gower, M. K. Clayton, D. S. Mackay, D. E. Ahl, J. M. Norman, and G. Diak. 2002. Application of geostatistics to characterize leaf area index (LAI) from flux tower to landscape scales using a cyclic sampling design. Ecosystems 5(7): 0667-0679.

Carlson, T. N., and D. A. Ripley. 1997. On the relation between NDVI, fractional vegetation cover, and leaf area index. Remote sensing of Environment 62(3): 241-252.

Chapin, F. S., A. D. McGuire, J. Randerson, R. Pielke, D. Baldocchi, S. E. Hobbie, N. Roulet, W. Eugster, E. Kasischke, E. B. Rastetter, S. A. Zimov, S. W. Running. 2000. Arctic and boreal ecosystems of western North America as components of the climate system. Global Change Biology 6(S1): 211-223.

Chen, J. M., & Black, T. A. 1992. Defining leaf area index for non-flat leaves. Plant, Cell & Environment, 15(4), 421-429.

Chen, J. M., & Cihlar, J. 1996. Retrieving leaf area index of boreal conifer forests using Landsat TM images. Remote sensing of Environment, 55(2), 153-162.

Chen, M., and Q. Zhuang. 2012. Spatially explicit parameterization of a terrestrial ecosystem model and its application to the quantification of carbon dynamics of forest ecosystems in the conterminous United States. Earth Interactions 16(5): 1-22.

Chen, M., Q. Zhuang, D. R. Cook, R. Coulter, M. Pekour, R. L. Scott, J.W. Munger, and K. Bible. 2011. Quantification of terrestrial ecosystem carbon dynamics in the conterminous United States combining a process-based biogeochemical model and MODIS and AmeriFlux data. Biogeosciences 8(2): 2721.

Chen, M., Zhuang, Q., Cook, D. R., Coulter, R., Pekour, M., Scott, R. L., Munger, J.W., & Bible, K. 2011. Quantification of terrestrial ecosystem carbon dynamics in the conterminous United States combining a process-based biogeochemical model and MODIS and AmeriFlux data. Biogeosciences, 8(2), 2721.

Chmielewski, F. M., and T. Rötzer. 2001. Response of tree phenology to climate change across Europe. Agricultural and Forest Meteorology 108(2): 101-112.

Chuine, I., P. Yiou, N. Viovy, B. Seguin, V. Daux, and E. L. R. Ladurie. 2004. Historical phenology: grape ripening as a past climate indicator. Nature 432(7015): 289-290.

Claverie, M., J. L. Matthews, E. F. Vermote, and C. O. Justice. 2016. A 30+ year AVHRR LAI and FAPAR climate data record: Algorithm description and validation. Remote Sensing 8(3): 263.

Comins, H. N. 1997. Analysis of nutrient-cycling dynamics, for predicting sustainability and CO 2-response of nutrient-limited forest ecosystems. Ecological modelling, 99(1), 51-69.

Dickinson, R. E., Shaikh, M., Bryant, R., & Graumlich, L. 1998. Interactive canopies for a climate model. Journal of Climate, 11(11), 2823-2836.

Dolman, A. J., & De Jeu, R. A. M. 2010. Evaporation in focus. Nature Geoscience, 3(5), 296-296.

Duchemin, B., Hadria, R., Erraki, S., Boulet, G., Maisongrande, P., Chehbouni, A., Escadafal, R., Ezzahar, J., Hoedjes, J. C. B., Kharrou, M. H., Khabba, S., Mougenot, B., Olioso, A., Rodriguez, J. C., & Simonneaux, V. 2006. Monitoring wheat phenology and irrigation in Central Morocco: On the use of relationships between evapotranspiration, crops coefficients, leaf area index and remotely-sensed vegetation indices. Agricultural Water Management, 79(1), 1-27.

Edwards, M., & Richardson, A. J. 2004. Impact of climate change on marine pelagic phenology and trophic mismatch. Nature, 430(7002), 881-884.

Entekhabi, D., Njoku, E. G., O'Neill, P. E., Kellogg, K. H., Crow, W. T., Edelstein, W. N., ... & Kimball, J. 2010. The soil moisture active passive (SMAP) mission. Proceedings of the IEEE, 98(5), 704-716.

Fang, H., Liang, S., & Kuusk, A. 2003. Retrieving leaf area index using a genetic algorithm with a canopy radiative transfer model. Remote Sensing of Environment, 85(3), 257-270.

Felzer, B., D. Kicklighter, J. Melillo, C. Wang, Q. Zhuang, and R. Prinn. 2004. Effects of ozone on net primary production and carbon sequestration in the conterminous United States using a biogeochemistry model. Tellus B 56(3): 230-248.

Fisher, J. B., Tu, K. P., & Baldocchi, D. D. 2008. Global estimates of the land–atmosphere water flux based on monthly AVHRR and ISLSCP-II data, validated at 16 FLUXNET sites. Remote Sensing of Environment, 112(3), 901-919.

Hagen, S. C., B. H. Braswell, E. Linder, S. Frolking, A. D. Richardson, and D. Y. Hollinger. 2006. Statistical uncertainty of eddy flux-based estimates of gross ecosystem carbon exchange at Howland Forest, Maine. Journal of Geophysical Research: Atmospheres 111(D8).

Hargreaves, G. H., & Allen, R. G. (2003). History and evaluation of Hargreaves evapotranspiration equation. Journal of Irrigation and Drainage Engineering, 129(1), 53-63.

Hastings, W. K. 1970. Monte Carlo sampling methods using Markov chains and their applications. Biometrika, 57(1), 97-109.

Heinsch, F. A., M. Zhao, S. W. Running, J. S. Kimball, R. R. Nemani, K. J. Davis, … and B. E. Law. 2006. Evaluation of remote sensing based terrestrial productivity from MODIS using regional tower eddy flux network observations. IEEE Transactions on Geoscience and Remote Sensing 7(44): 1908-1925.

Henze, D. K., & Seinfeld, J. H. 2006. Development of the adjoint of GEOS-Chem. Atmospheric Chemistry and Physics Discussions, 6(5), 10591-10648.

Hurley, M. A., M. Hebblewhite, J. M. Gaillard, S. Dray, K. A. Taylor, W. K. Smith, P. Zager, and C. Bonenfant. 2014. Functional analysis of Normalized Difference Vegetation Index curves reveals overwinter mule deer survival is driven by both spring and autumn phenology. Philosophical Transactions of the Royal Society B 369(1643).

Intergovernmental Panel on Climate Change. 2014. Climate Change 2014–Impacts, Adaptation and Vulnerability: Regional Aspects. Cambridge University Press.

Jensen, M. E., & Haise, H. R. 1963. Estimating evapotranspiration from solar radiation. Proceedings of the American Society of Civil Engineers, Journal of the Irrigation and Drainage Division, 89, 15-41.

Jin, H., and L. Eklundh. 2014. A physically based vegetation index for improved monitoring of plant phenology. Remote Sensing of Environment 152: 512-525.

Johns, T. C., Carnell, R. E., Crossley, J. F., Gregory, J. M., Mitchell, J. F., Senior, C. A., ... & Wood, R. A. 1997. The second Hadley Centre coupled ocean-atmosphere GCM: model description, spinup and validation. Climate dynamics, 13(2), 103-134.

Jung, M., Reichstein, M., Ciais, P., Seneviratne, S. I., Sheffield, J., Goulden, M. L., ... & Dolman, A. J. 2010. Recent decline in the global land evapotranspiration trend due to limited moisture supply. Nature, 467(7318), 951-954.

Katul, G. G., Oren, R., Manzoni, S., Higgins, C., & Parlange, M. B. 2012. Evapotranspiration: A process driving mass transport and energy exchange in the soil-plant-atmosphere-climate system. Reviews of Geophysics, 50(3).

Keenan, T. F., J. Gray, M. A. Friedl, M. Toomey, G. Bohrer, D. Y. Hollinger, … and B. Yang. 2014. Net carbon uptake has increased through warming-induced changes in temperate forest phenology. Nature Climate Change 4(7): 598-604.

King, D. A. 1995. Equilibrium analysis of a decomposition and yield model applied to Pinus radiata plantations on sites of contrasting fertility. Ecological modelling, 83(3), 349-358.

Kwon, E. Y., & Primeau, F. 2006. Optimization and sensitivity study of a biogeochemistry ocean model using an implicit solver and in situ phosphate data. Global biogeochemical cycles, 20(4).

Liang, L., M. D. Schwartz, Z. Wang, F. Gao, C. B. Schaaf, B. Tan, … and X. Zhang. 2014. A cross comparison of spatiotemporally enhanced springtime phenological measurements from satellites and ground in a northern US mixed forest. IEEE Transactions on Geoscience and Remote Sensing 52(12): 7513-7526.

Liang, S., X. Zhao, S. Liu, W. Yuan, X. Cheng, Z. Xiao, X. Zhang, Q. Liu, J. Cheng, H. Tang, Y. Qu, Y. Bo, H. Ren, K. Yu, and J. Townshend. 2013. A long-term Global LAnd Surface Satellite (GLASS) data-set for environmental studies. International Journal of Digital Earth 6(sup1): 5-33.

Linkosalo, T., H. K. Lappalainen, and P. Hari. 2008. A comparison of phenological models of leaf bud burst and flowering of boreal trees using independent observations. Tree Physiology 28(12): 1873-1882.

Liu, S., Chen, M., & Zhuang, Q. 2016. Direct radiative effects of tropospheric aerosols on changes of global surface soil moisture. Climatic Change, 1-13.

Liu, Y., Q. Zhuang, D. Miralles, Z. Pan, D. Kicklighter, Q. Zhu, Y. He, J. Chen, N. Tchebakova, A. Sirin, D. Niyogi, and J. Melillo. 2015. Evapotranspiration in Northern Eurasia: Impact of forcing uncertainties on terrestrial ecosystem model estimates. Journal of Geophysical Research Atmospheres 120(7): 2647-2660.

Liu, Y., Q. Zhuang, M. Chen, Z. Pan, N. Tchebakova, A. Sokolov, and Y. He. 2013. Response of evapotranspiration and water availability to changing climate and land cover on the Mongolian Plateau during the 21st century. Global and Planetary Change 108: 85-99.

Liu, Y., Zhuang, Q., Miralles, D., Pan, Z., Kicklighter, D., Zhu, Q., He, Y., Chen, J., Tchebakova, N., Sirin, A., Niyogi, D., & Melillo, J. 2015. Evapotranspiration in Northern Eurasia: Impact of forcing uncertainties on terrestrial ecosystem model estimates. Journal of Geophysical Research: Atmospheres, 120(7), 2647-2660.

Liu, Y., Zhuang, Q., Pan, Z., Miralles, D., Tchebakova, N., Kicklighter, D., ... & Melillo, J. 2014. Response of evapotranspiration and water availability to the changing climate in Northern Eurasia. Climatic change, 126(3-4), 413-427.

Lu, H., M. R. Raupach, T. R. McVicar, and D. J. Barrett. 2003. Decomposition of vegetation cover into woody and herbaceous components using AVHRR NDVI time series. Remote Sensing of Environment 86(1): 1-18.

Lu, X., & Zhuang, Q. 2010. Evaluating evapotranspiration and water-use efficiency of terrestrial ecosystems in the conterminous United States using MODIS and AmeriFlux data. Remote Sensing of Environment, 114(9), 1924-1939.

Luo, Y., K. Ogle, C. Tucker, S. Fei, C. Gao, S. LaDeau, J. S. Clark, and D. S. Schimel. 2011. Ecological forecasting and data assimilation in a data-rich era. Ecological Applications 21(5): 1429-1442.

McGuire, A. D., J. M. Melillo, L. A. Joyce, D. W. Kicklighter, A. L. Grace, B. I. I. I. Moore, and C. J. Vorosmarty. 1992. Interactions between carbon and nitrogen dynamics in estimating net primary productivity for potential vegetation in North America. Global Biogeochemical Cycles 6(2): 101-124.

Melaas, E. K., D. Sulla-Menashe, J. M. Gray, T. A. Black, T. H. Morin, A. D. Richardson, and M. A. Friedl. 2016. Multisite analysis of land surface phenology in North American temperate and boreal deciduous forests from Landsat. Remote Sensing of Environment 186: 452-464.

Melillo, J. M., A. D. McGuire, D. W. Kicklighter, B. Moore, C. J. Vorosmarty, and A. L. Schloss. 1993. Global climate change and terrestrial net primary production. Nature 363(6426): 234-240.

Menzel, A., and P. Fabian. 1999. Growing season extended in Europe. Nature 397(6721): 659-659.

Metropolis, N., A. W. Rosenbluth, M. N. Rosenbluth, A. H. Teller, and E. Teller. 1953. Equation of state calculations by fast computing machines. The journal of chemical physics 21(6): 1087-1092.

Michalakes, J., & Vachharajani, M. 2008. GPU acceleration of numerical weather prediction. Parallel Processing Letters, 18(04), 531-548.

Miralles, D. G., De Jeu, R. A., Gash, J. H., Holmes, T. R., & Dolman, A. J. 2011. Magnitude and variability of land evaporation and its components at the global scale. Hydrology and Earth System Sciences.

Monteith, J. L. 1965. Evaporation and environment. In Symp. Soc. Exp. Biol(Vol. 19, No. 205-23, p. 4).

Mooney, H., Cropper, A., & Reid, W. 2005. Confronting the human dilemma. Nature, 434(7033), 561-562.

Mu, Q., F. A. Heinsch, M. Zhao, and S. W. Running. 2007. Development of a global evapotranspiration algorithm based on MODIS and global meteorology data. Remote Sensing of Environment 111(4): 519-536.

Mu, Q., Zhao, M., & Running, S. W. 2011. Improvements to a MODIS global terrestrial evapotranspiration algorithm. Remote Sensing of Environment, 115(8), 1781-1800.

Myneni, R. B., C. D. Keeling, C. J. Tucker, G. Asrar, and R. R. Nemani. 1997. Increased plant growth in the northern high latitudes from 1981-1991. Nature. 386: 698-701.

Myneni, R. B., Nemani, R. R., & Running, S. W. (1997). Algorithm for the estimation of global land cover, LAI and FPAR based on radiative transfer models. IEEE Trans. Geosci. Remote Sens, 35(6), 1380-1393.

Nvidia, C. (2007). NVIDIA CUDA Compute Unified Device Architecture Programming Guide. NVIDIA Corporation.

Pan, S., Tian, H., Dangal, S. R., Yang, Q., Yang, J., Lu, C., ... & Ouyang, Z. (2015). Responses of global terrestrial evapotranspiration to climate change and increasing atmospheric CO2 in the 21st century. Earth's Future, 3(1), 15-35.

Pan, Y., MCGUIRE, A. D., KICKLIGHTER, D. W., & MELILLO, J. M. (1996). The importance of climate and soils for estimates of net primary production: a sensitivity analysis with the terrestrial ecosystem model. Global Change Biology, 2(1), 5-23.

Qu, Y., & Zhuang, Q. (2018). Modeling leaf area index in North America using a process-based terrestrial ecosystem model. Ecosphere, 9(1).

Raich, J. W., and W. H. Schlesinger. 1992. The global carbon dioxide flux in soil respiration and its relationship to vegetation and climate. Tellus B 44(2): 81-99.

Raich, J. W., E. B. Rastetter, J. M. Melillo, D. W. Kicklighter, P. A. Steudler, B. J. Peterson, … and C. J. Vorosmarty. 1991. Potential net primary productivity in South America: application of a global model. Ecological Applications 1(4): 399-429.

Rasmusson, E. M. (1968). Atmospheric water vapor transport and the water balance of North America: II. Large-scale water balance investigations. Monthly Weather Review, 96(10), 720-734.

Raupach, M. R., P. J. Rayner, D. J. Barrett, R. S. DeFries, M. Heimann, D. S. Ojima, S. Quegan, and C. C. Schmullius. 2005. Model-data synthesis in terrestrial carbon observation: methods, data requirements and data uncertainty specifications. Global Change Biology 11(3): 378-397.

Riahi, K., Grübler, A., & Nakicenovic, N. (2007). Scenarios of long-term socio-economic and environmental development under climate stabilization. Technological Forecasting and Social Change, 74(7), 887-935.

Ricciuto, D. M., Davis, K. J., & Keller, K. (2008). A Bayesian calibration of a simple carbon cycle model: The role of observations in estimating and reducing uncertainty. Global biogeochemical cycles, 22(2).

Ricciuto, D. M., M. P. Butler, K. J. Davis, B. D. Cook, P. S. Bakwin, A. Andrews, and R. M. Teclaw. 2008. Causes of interannual variability in ecosystem-atmosphere CO2 exchange in a northern Wisconsin forest using a Bayesian model calibration. Agricultural and Forest Meteorology 148(2): 309-327.

Richardson, A. D., R. S. Anderson, M. A. Arain, A. G. Barr, G. Bohrer, G. Chen, … and M. C. Dietze. 2012. Terrestrial biosphere models need better representation of vegetation phenology: results from the North American Carbon Program Site Synthesis. Global Change Biology 18(2): 566-584.

Rigden, A. J., & Salvucci, G. D. (2016). Stomatal response to humidity and CO2 implicated in recent decline in US evaporation. Global change biology.

Rodriguez-Galiano, V. F., M. Sanchez-Castillo, J. Dash, P. M. Atkinson, and J. Ojeda-Zujar. 2016. Modelling interannual variation in the spring and autumn land surface phenology of the European forest. Biogeosciences 13(11): 3305-3317.

Seager, R., M. Ting, I. Held, Y. Kushnir, J. Lu, G. Vecchi, H. Huang, N. Harnik, A. Leetmaa, N. Lau, C. Li, J. Velez, and N. Naik. 2007. Model projections of an imminent transition to a more arid climate in southwestern North America. Science 316(5828): 1181-1184.

Sobrino, J. A., Gómez, M., Jiménez-Muñoz, J. C., Olioso, A., & Chehbouni, G. (2005). A simple algorithm to estimate evapotranspiration from DAIS data: Application to the DAISEX campaigns. Journal of hydrology, 315(1), 117-125.

Song, L., Zhuang, Q., Yin, Y., Zhu, X., & Wu, S. (2017). Spatio-temporal dynamics of evapotranspiration on the Tibetan Plateau from 2000 to 2010. Environmental Research Letters, 12(1), 014011.

Sulman, B. N., A. R. Desai, B. D. Cook, N. Saliendra, and D. S. Mackay. 2009. Contrasting carbon dioxide fluxes between a drying shrub wetland in Northern Wisconsin, USA, and nearby forests. Biogeosciences 6(6): 1115-1126.

Sun, G., Alstad, K., Chen, J., Chen, S., Ford, C. R., Lin, G., ... & Noormets, A. (2011). A general predictive model for estimating monthly ecosystem evapotranspiration. Ecohydrology, 4(2), 245-255.

Sung, S., and R. M. Amasino. 2004. Vernalization in Arabidopsis thaliana is mediated by the PHD finger protein VIN3. Nature 427(6970): 159-164.

Tang, J., and Q. Zhuang. 2009. A global sensitivity analysis and Bayesian inference framework for improving the parameter estimation and prediction of a process-based Terrestrial Ecosystem Model. Journal of Geophysical Research: Atmospheres 144(D15).

Thornton, P. E., & Rosenbloom, N. A. (2005). Ecosystem model spin-up: estimating steady state conditions in a coupled terrestrial carbon and nitrogen cycle model. Ecolo

Urbanski, S., C. Barford, S. Wofsy, C. Kucharik, E. Pyle, J. Budney, K. McKain, D. Fitzjarrald, M. Czikowsky, and J. W. Munger. 2007. Factors controlling CO2 exchange on timescales from hourly to decadal at Harvard Forest. Journal of Geophysical Research: Biogeosciences 112(G2).

Van Vuuren, D. P., Den Elzen, M. G., Lucas, P. L., Eickhout, B., Strengers, B. J., Van Ruijven, B., ... & van Houdt, R. (2007). Stabilizing greenhouse gas concentrations at low levels: an assessment of reduction strategies and costs. Climatic Change, 81(2), 119-159.

Vörösmarty, C. J., C. A. Federer, and A. L. Schloss. 1998. Potential evaporation functions compared on US watersheds: Possible implications for global-scale water balance and terrestrial ecosystem modeling. Journal of Hydrology 207(3-4): 147-169.

Vörösmarty, C. J., Green, P., Salisbury, J., & Lammers, R. B. (2000). Global water resources: vulnerability from climate change and population growth. science, 289(5477), 284-288.

Vörösmarty, C. J., P. B. McIntyre, M. O. Gessner, D. Dudgeon, A. Prusevich, P. Green, S. Glidden et al. 2010. Global threats to human water security and river biodiversity. Nature 467(7315): 555-561.

Wang, K., and R. E. Dickinson. 2012. A review of global terrestrial evapotranspiration: Observation, modeling, climatology, and climatic variability. Reviews of Geophysics 50(2).

Wang, K., Wang, P., Li, Z., Cribb, M., & Sparrow, M. (2007). A simple method to estimate actual evapotranspiration from a combination of net radiation, vegetation index, and temperature. Journal of Geophysical Research: Atmospheres, 112(D15).

Wiegand, C. L., A. J. Richardson, and E. T. Kanemasu. 1979. Leaf area index estimates for wheat from Landsat and their implications for evapotranspiration and crop modeling. Agronomy Journal 71(2): 336-342.

Wilson, K. B., & Baldocchi, D. D. (2000). Seasonal and interannual variability of energy fluxes over a broadleaved temperate deciduous forest in North America. Agricultural and Forest Meteorology, 100(1), 1-18.

Wilson, P. J., K. E. N. Thompson, and J. G. Hodgson. 1999. Specific leaf area and leaf dry matter content as alternative predictors of plant strategies. New phytologist 143(1): 155-162.

Xia, J. Y., Luo, Y. Q., Wang, Y. P., Weng, E. S., & Hararuk, O. (2012). A semi-analytical solution to accelerate spin-up of a coupled carbon and nitrogen land model to steady state. Geoscientific Model Development, 5(5), 1259-1271.

Xiu, D., & Hesthaven, J. S. (2005). High-order collocation methods for differential equations with random inputs. SIAM Journal on Scientific Computing, 27(3), 1118-1139.

Xiu, D., & Karniadakis, G. E. (2002). The Wiener--Askey polynomial chaos for stochastic differential equations. SIAM journal on scientific computing, 24(2), 619-644.

Xu, T., L. White, D. Hui, and Y. Luo. 2006. Probabilistic inversion of a terrestrial ecosystem model: Analysis of uncertainty in parameter estimation and model prediction. Global Biogeochemical Cycles 20(2).

Yue, X., N. Unger, X. Zhang, and C. S. Vogel. 2015. Probing the past 30-year phenology trend of US deciduous forests. Biogeosciences 12(4693)

Zhang, X., D. Tarpley, and J. T. Sullivan. 2007. Diverse responses of vegetation phenology to a warming climate. Geophysical Research Letters 34(19).

Zhang, X., Friedl, M. A., Schaaf, C. B., Strahler, A. H., Hodges, J. C., Gao, F., Reed, B. C., & Huete, A. (2003). Monitoring vegetation phenology using MODIS. Remote sensing of environment, 84(3), 471-475.

Zhang, X., M. A. Friedl, C. B. Schaaf, A. H. Strahler, J. C. Hodges, F. Gao, B. C. Reed, and A. Huete. 2003. Monitoring vegetation phenology using MODIS. Remote Sensing of Environment 84(3): 471-475.

Zhang, Y., J. L. Arancibia, T. R. McVicar, F. H. Chiew, J. Vaze, C. Liu, X. Lu, H. Zheng, Y. Wang, Y. Y. Liu, D. G. Miralles, and M. Pan. 2016. Multi-decadal trends in global terrestrial evapotranspiration and its components. Scientific reports 6.

Zhang, Y., Peña-Arancibia, J. L., McVicar, T. R., Chiew, F. H., Vaze, J., Liu, C., ... & Miralles, D. G. (2016). Multi-decadal trends in global terrestrial evapotranspiration and its components. Scientific reports, 6.

Zhu, Q., and Q. Zhuang. 2013. Improving the quantification of terrestrial ecosystem carbon dynamics over the United States using an adjoint method. Ecosphere 4(10): 1-21.

Zhu, Q., Zhuang, Q., Henze, D., Bowman, K., Chen, M., Liu, Y., ... & Oechel, W. (2014). Constraining terrestrial ecosystem CO 2 fluxes by integrating models of biogeochemistry and atmospheric transport and data of surface carbon fluxes and atmospheric CO 2 concentrations. Atmospheric Chemistry and Physics Discussions, 14(16), 22587-22638.

Zhuang, Q., J. He, Y. Lu, L. Ji, J. Xiao, and T. Luo. 2010. Carbon dynamics of terrestrial ecosystems on the Tibetan Plateau during the 20th century: an analysis with a process-based biogeochemical model. Global Ecology and Biogeography 19(5): 649-662.

Zhuang, Q., A. D. McGuire, J. M. Melillo, J. S. Clein, R. J. Dargaville, D. W. Kicklighter, R. B. Myneni, J. Dong, V. E. Romanovsky, J. Harden, and J. E. Hobbie. 2003. Carbon cycling in extratropical terrestrial ecosystems of the Northern Hemisphere during the 20th century: a modeling analysis of the influences of soil thermal dynamics. Tellus B 55(3): 751-776.

Zhuang, Q., A. D. McGuire, K. P. O'neill, J. W. Harden, V. E. Romanovsky, and J. Yarie. 2002. Modeling soil thermal and carbon dynamics of a fire chronosequence in interior Alaska. Journal of Geophysical Research: Atmospheres 107(D1)

Zhuang, Q., V. E. Romanovsky, and A. D. McGuire. 2001. Incorporation of a permafrost model into a large-scale ecosystem model: Evaluation of temporal and spatial scaling issues in simulating soil thermal dynamics. Journal of Geophysical Research: Atmospheres 106(D24): 33649-33670

Zomer, R. J., Trabucco, A., Bossio, D. A., & Verchot, L. V. (2008). Climate change mitigation: A spatial analysis of global land suitability for clean development mechanism afforestation and reforestation. Agriculture, ecosystems & environment, 126(1), 67-80.